inhibitor with the i.v. administration of Resovist® or the PEG–PAsp-coated magnetite nanoparticles on their imaging capability in size-matched xenografts of the BxPC3 cell line. Fig. 6A shows the T_2-weighted MR images of the tumors at different time periods after the intravenous administration (preinjection, and 1 and 2 h postinjection) of PEG–PAsp-coated magnetite nanoparticles with and without TGF-β inhibitor.

Resovist® failed to image the tumor even with the co-administration of TGF-β inhibitor, presumably due to the non-specific accumulation into the reticuloendothelial system [8]. In contrast, the PEG–PAsp-coated magnetite nanoparticles exhibited significant negative enhancement of signal intensity in the tumor region of T_2-weighted images when combined with TGF-β inhibitor, suggesting the accumulation of detectable amounts of the PEG–PAsp-coated magnetite nanoparticles within 2 h after injection. Therefore, the difference in behavior of these two types of magnetite nanoparticles *in vivo* had a crucial importance in achieving effective tumor accumulation for successful MR imaging.

To further verify the accumulation of iron oxide nanoparticles in the tumor, we performed Prussian blue staining of the tumor tissues to detect iron oxide, which stains blue. As shown in Fig. 6B, positive staining of the tumor for iron oxide was only obvious in the condition with PEG–PAsp-coated nanoparticles combined with the TGF-β inhibitor. Areas of iron staining in the tumor were then quantified as seen in Fig. 6D, demonstrating a significant increase in the areas of positive staining by TGF-β inhibitor treatment. The presence of iron oxide was consistent with the MRI results. Iron oxide was observed in the area rich in fibrotic components, suggesting that the administration of TGF-β inhibitor transiently increases the permeability of the tumor capillary to promote the extravasation of the PEG–PAsp-coated magnetite nanoparticles, even though the BxPC3 tumor has the characteristic of hypovascularity [11].

Lastly, we examined liver tissues from the mice treated with Resovist® or the PEG–PAsp-coated magnetite nanoparticle, with or without TGF-β inhibitor, by iron staining (Fig. 6C). Although aggregates of Resovist® accumulated in the liver, particularly in cells with smaller nuclei (presumably Kuppfer cells), far less PEG–PAsp-coated magnetite nanoparticles accumulated in the liver without aggregation. These results did not differ with or without TGF-β inhibitor, which was determined by the area of Prussian blue staining (Fig. 6E).

4. Conclusion

In conclusion, we here demonstrated the physicochemical properties of PEG–PAsp-coated magnetite nanoparticles and the feasibility of these nanoparticles as MR contrast agents for cancer diagnosis. Improving the stability of nanoparticles might be important for enabling a longer half-life in the bloodstream and a better accumulation in tumor tissue, leading to effective MR imaging with contrast agents. The neutral ζ-potential of the PEG–PAsp-coated nanoparticle may contribute to avoidance of reticuloendothelial system uptake. Formation of the stable and dense PEG layer on the magnetite surface through the anchoring of PEG–PAsp by the monodentate chelation of COO^- residues to iron atoms definitely plays a substantial role in the increased stability of the nanoparticles *in vivo*. The use of PEG–PAsp-coated magnetite nanoparticles combined with a TGF-β inhibitor could thus become a novel regime in the diagnosis of intractable cancers, including pancreatic adenocarcinoma.

Acknowledgements

The authors thank Dr James R. Christie II, The University of Tokyo, for editing the English of the manuscript. This work was supported by a Grant-in-Aid for Scientific Research from the Ministry of Education, Culture, Sports, Science and Technology (MEXT), Core Research for Evolution of Science and Technology (CREST), Japan Science and Technology Corporation (JST), and the 21st century COE program 'Human-Friendly Materials based on Chemistry' from MEXT.

Appendix A. Supplementary data

Supplementary data associated with this article can be found, in the online version, at doi:10.1016/j.jconrel.2009.06.002.

References

[1] M.R. Dreher, W. Liu, C.R. Michelich, M.W. Dewhirst, F. Yuan, A. Chilkoti, Tumor vascular permeability, accumulation, and penetration of macromolecular drug carriers, J. Natl. Cancer Inst. 98 (5) (2006) 335–344.
[2] H.A. Burris, M.J. Moore, J. Andersen, M.R. Green, M.L. Rothenberg, M.R. Modiano, M.C. Cripps, R.K. Portenoy, A.M. Storniolo, P. Tarassoff, R. Nelson, F.A. Dorr, C.D. Stephens, D.D. Von Hoff, Improvements in survival and clinical benefit with gemcitabine as first-line therapy for patients with advanced pancreas cancer: a randomized trial, J. Clin. Oncol. 15 (6) (1997) 2403–2413.
[3] D.V. Sahani, Z.K. Shah, O.A. Catalano, G.W. Boland, W.R. Brugge, Radiology of pancreatic adenocarcinoma: current status of imaging, J. Gastroenterol. Hepatol. 23 (1) (2008) 23–33.
[4] D.L. Huber, Synthesis, properties, and applications of iron nanoparticles, Small 1 (5) (2005) 482–501.
[5] R. Weissleder, G. Elidonzo, J. Wittenberg, C.A. Rabito, H.H. Bengele, L. Josephson, Ultrasmall superparamagnetic iron oxide: characterization of a new class of contrast agents for MR imaging, Radiology 175 (2) (1990) 489–493.
[6] M. Lewin, N. Carlesso, C.H. Tung, X.W. Tang, D. Cory, D.T. Scadden, R. Weissleder, Tat peptide-derivatized magnetic nanoparticles allow *in vivo* tracking and recovery of progenitor cells, Nat. Biotechnol. 18 (4) (2000) 410–414.
[7] Y.W. Jun, J.H. Lee, J. Cheon, Chemical design of nanoparticle probes for high-performance magnetic resonance imaging, Angew. Chem. Int. Ed. 47 (28) (2008) 5122–5135.
[8] D.D. Stark, R. Weissleder, G. Elizondo, et al., Superparamagnetic iron oxide: clinical application as a contrast agent for MR imaging of the liver, Radiology 168 (2) (1988) 297–301.
[9] T. Neuberger, B. Schöpf, H. Hofmann, M. Hofmann, B. von Rechenberg, Super-paramagnetic nanoparticles for biomedical applications: possibilities and limitations of a new drug delivery system, J. Magn. Mater. 293 (1) (2005) 483–496.
[10] M. Kumagai, Y. Imai, T. Nakamura, Y. Yamasaki, M. Sekino, S. Ueno, K. Hanaoka, K. Kikuchi, T. Nagano, E. Kaneko, K. Shimokado, K. Kataoka, Iron hydroxide nanoparticles coated with poly(ethylene glycol)–poly(aspartic acid) block copolymer as novel magnetic resonance contrast agents for *in vivo* cancer imaging, Colloids Surf. B: Biointerfaces 56 (1–2) (2007) 174–181.
[11] M.R. Kano, Y. Bae, C. Iwata, Y. Morishita, M. Yashiro, M. Oka, T. Fujii, A. Komuro, K. Kiyono, M. Kaminishi, K. Hirakawa, Y. Ouchi, N. Nishiyama, K. Kataoka, K. Miyazono, Improvement of cancer-targeting therapy, using nanocarriers for intractable solid tumors by inhibition of TGF-β signaling, Proc. Natl. Acad. Sci. U. S. A. 104 (9) (2007) 3460–3465.
[12] Y. Matsumura, H. Maeda, A new concept for macromolecular therapeutics in cancer-chemotherapy-mechanism of tumoritropic accumulation of proteins and the antitumor agent SMANCS, Cancer Res. 46 (12) (1986) 6387–6392.
[13] N. Nishiyama, M. Yokoyama, T. Aoyagi, T. Okano, Y. Sakurai, K. Kataoka, Preparation and characterization of self-assembled polymer-metal complex micelle from cis-dichlorodiammineplatinum(II) and poly(ethylene glycol)–poly(alpha,beta-aspartic acid) block copolymer in an aqueous medium, Langmuir 15 (2) (1999) 377–383.
[14] E. Fukushima, S.B.W. Roeder (Eds.), Experimental pulse NMR: a nuts and bolts approach, Addison-Wesley, Reading, Mass, 1981, pp. 28–35.
[15] A.J.S. MacFadzean, L.J. Davis, Iron-staining erythrocytic inclusions with especial reference to acquired haemolytic anaemia, Glasgow Med. J. 28 (1947) 237–279.
[16] S. Takae, Y. Akiyama, H. Otsuka, T. Nakamura, Y. Nagasaki, K. Kataoka, Ligand density effect on biorecognition by PEGylated gold nanoparticles: regulated interaction of RCA120 lectin with lactose installed to the distal end of tethered PEG strands on gold surface, Biomacromolecules 6 (2) (2005) 818–824.
[17] L. Cromières, V. Moulin, B. Fourest, E. Giffaut, Physico-chemical characterization of the colloidal hematite/water interface: experimentation and modeling, Colloids Surf., A. Physicochem. Eng. Asp. 202 (1) (2002) 101–115.
[18] L.J. Kirwan, P.D. Fawell, W. van Bronswijk, In situ FTIR-ATR examination of poly (acrylic acid) adsorbed onto hematite at low pH, Langmuir 19 (14) (2003) 5802–5807.
[19] Y.X.J. Wang, S.M. Hussain, G.P. Krestin, Superparamagnetic iron oxide contrast agents: physicochemical characteristics and applications in MR imaging, Eur. Radiol. 11 (11) (2001) 2319–2331.
[20] S.R. Wan, J.S. Huang, M. Guo, H. Zhang, Y. Cao, H. Yan, K. Liuet, Biocompatible superparamagnetic iron oxide nanoparticle dispersions stabilized with poly (ethylene glycol)oligo(aspartic acid) hybrids, J. Biomed. Mater. Res. A 80A (4) (2007) 946–954.
[21] C.W. Jung, Surface-properties of superparamagnetic iron-oxide MR contrast agents — ferumoxides, ferumoxtran, ferumoxsil, Magn. Reson. Imaging 13 (5) (1995) 675–691.

Enhanced Percolation and Gene Expression in Tumor Hypoxia by PEGylated Polyplex Micelles

Muri Han[1], Makoto Oba[2], Nobuhiro Nishiyama[3,4], Mitsunobu R Kano[4,5], Shinae Kizaka-Kondoh[6] and Kazunori Kataoka[1,3,4,7]

[1]Department of Materials Engineering, Graduate School of Engineering, The University of Tokyo, Tokyo, Japan; [2]Department of Clinical Vascular Regeneration, Graduate School of Medicine, The University of Tokyo, Tokyo, Japan; [3]Center for Disease Biology and Integrative Medicine, Graduate School of Medicine, The University of Tokyo, Tokyo, Japan; [4]Center for NanoBio Integration, The University of Tokyo, Tokyo, Japan; [5]Department of Molecular Pathology, Graduate School of Medicine, The University of Tokyo, Tokyo, Japan; [6]Department of Radiation Oncology and Image-Applied Therapy, Kyoto University, Graduate School of Medicine, Kyoto, Japan; [7]Core Research for Evolutional Science and Technology (CREST), Japan Science and Technology Agency (JST), Kawaguchi, Japan

In regard to gene vectors for cancer gene therapy, their percolation into the tumor tissue should be essential for successful outcome. Here, we studied the tumor penetrability of nonviral vectors (polyplexes) after incubation with the multicellular tumor spheroid (MCTS) models and intratumoral (i.t.) injection into subcutaneous tumors. As a result, polyethylene glycolated (PEGylated), core–shell type polyplexes (polyplex micelles) showed facilitated percolation and improved transfection inside the tumor tissue, whereas conventional polyplexes from cationic polymers exhibited limited percolation and localized transfection. Furthermore, the transfection of hypoxia-responsive plasmid demonstrated that polyplex micelles allowed the transfection to the hypoxic region of the tumor tissue in both *in vitro* and *in vivo* experiments. To the best of our knowledge, our results demonstrated for the first time that polyplex micelles might show improved tumor penetrability over cationic polyplexes, thereby achieving transfection into the inside of the tumor tissue.

Received 22 December 2008; accepted 24 April 2009; published online 26 May 2009. doi:10.1038/mt.2009.119

INTRODUCTION

Gene therapy is a promising method for the treatment of malignant tumors, and its success relies on the capabilities of gene vectors. In this regard, nonviral vectors composed of plasmid DNA (pDNA) and cationic polymers, so-called polyplexes have been attracting much attention due to several advantages such as no immunogenicity, safety, and easy large-scale preparation.[1–4] So far, considerable efforts have been devoted to improve the transfection efficiency of polyplexes as well as control the gene expression in the body.[5–8] However, in regard to gene vectors for cancer gene therapy, much attention should be paid on another important property: percolation into the tumor tissue. In general, solid tumors are known to possess heterogeneous structures composed of blood vessels, interstitial tissues, clusters of tumor cells with normoxic and hypoxic regions. Therefore, it might be difficult to deliver the therapeutic agents to tumor cells distant from the vasculature.[9–11] Furthermore, hypoxic region induced by the insufficient blood supply is known to be inherently less susceptible to therapeutic agents.[10] As such difficulty in treating hypoxic regions is often correlated with recurrence and malignant progression of solid tumors,[10] overcoming the limited drug access to hypoxic cells should be a critical issue in cancer therapy. Thus, the percolation of gene vectors in solid tumors should be of primary importance to achieve successful cancer gene therapy.

Recently, we have developed a highly transfectable but less-toxic core–shell type polyplex with poly(ethylene glycol) (PEG) palisades (polyplex micelle), which was formed through the electrostatic interaction between pDNA and PEG-*b*-polyaspartamide having 1,2-diaminoethane side chain (PEG-*b*-P[Asp(DET)]) (Figure 1).[12,13] This polyplex micelle showed remarkable features, including efficient gene transfer to primary cells,[12] successful *in vivo* transfection to a rabbit carotid artery,[14] and transfection-mediated bone regeneration.[15] In this study, we explored the tumor penetrability of polyplex micelles, because we have recently demonstrated that amphiphilic block copolymer micelles can show penetrability into multicellular tumor spheroids (MCTSs)[16] as well as solid tumors after intravenous administration.[17] Here, we demonstrated that polyplex micelles from PEG-*b*-P[Asp(DET)] showed successful transfection to hypoxic cells inside MCTS as well as enhanced percolation and widely distributed gene expression within the tumor tissue after intratumoral (i.t.) injection. In contrast, cationic polyplexes showed limited penetration and localized transfection in both *in vitro* and *in vivo* studies. These results suggest that polyplex micelles may overcome the transport barrier of nonviral vectors, facilitating their use for cancer gene therapy.

RESULTS

Transfection to MCTS

MCTS is an appropriate *in vitro* tumor model representing morphological and functional features of *in vivo* avascular solid tumors, and is composed of actively proliferating outer cell layers

Correspondence: *Kazunori Kataoka, Department of Materials Engineering, Graduate School of Engineering, The University of Tokyo, 7-3-1 Hongo, Bunkyo-ku, Tokyo 113-8656, Japan. E-mail: kataoka@bmw.t.u-tokyo.ac.jp*

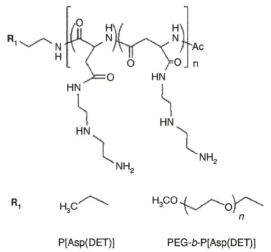

Figure 1 Chemical structures of P[Asp(DET)] homopolymers and PEG-*b*-P[Asp(DET)] block copolymers.

and hypoxic and quiescent inner cells.[18] In this study, a large-sized MCTS (400–500 μm), which possessed a hypoxic region characterized by necrotic cells inside due to limited supply of oxygen and nutrition (Figure 2a), was transfected with pCAcc + *Venus* by using the linear polyethylenimine (LPEI) and P[Asp(DET)] polyplexes and PEG-*b*-P[Asp(DET)] polyplex micelles at a defined mixing ratio of the number of amino groups units to a nucleotide unit (N/P ratio). Note that, although we have recently reported that a small-sized MCTS (~100 μm) can be disrupted by the cytotoxicity of polyplexes,[19] the large-sized MCTS used in this study is stable against the polyplex-mediated transfection. The expression of a variant of yellow fluorescent protein, *Venus* was evaluated by confocal microscopic observation. At 48 hours after the transfection (24-hour incubation and additional 24-hour incubation after the medium replacement), the LPEI polyplexes (N/P = 6, the manufacturer's recommendation ratio) and P[Asp(DET)] polyplexes (N/P = 20) showed significant gene expression limited to the periphery of the MCTS (Figure 2b). This result indicates that cationic polyplexes might lack the ability to transfect the inside of the MCTS. In contrast, PEG-*b*-P[Asp(DET)] polyplex micelles (N/P = 20) showed appreciable gene expression at not only the periphery but also the inside of the MCTS (Figure 2b), where a great number of necrotic cells were observed as indicated by red fluorescence from ethidium homodimer (EthD-1) (Figure 2c). These results suggest that polyplex micelles may allow the gene transfer to tumor cells in the hypoxic inner region of the MCTS.

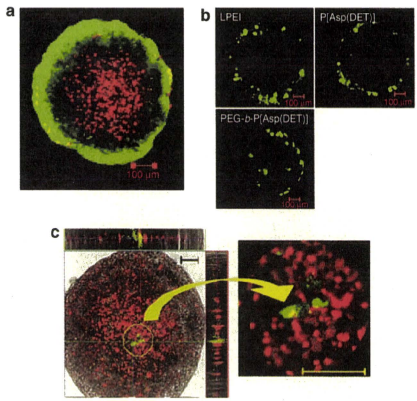

Figure 2 Transfection to HuH-7 MCTS. (**a**) Live/dead staining of HuH-7 spheroid (optical slice at the middle of spheroid. Bar = 100 μm). The green and red fluorescence are derived from live and dead cells, respectively. (**b**) Gene expression of pCAcc + *Venus* in HuH-7 MCTS transfected with LPEI polyplexes (N/P = 6), P[Asp(DET)] polyplexes (N/P = 20), and PEG-*b*-P[Asp(DET)] polyplex micelles (N/P = 20) (24 hours of incubation time and 24 hours of additional incubation after the medium replacement). (**c**) Gene expression of pCAcc + *Venus* at the inner region of HuH-7 MCTS transfected with PEG-*b*-P[Asp(DET)] polyplex micelles (N/P = 20) (24 hours of incubation time and 24 hours of additional incubation after the medium replacement) (Left: The red and green fluorescence are derived from dead cells and transfected protein *Venus*, respectively. Right: Magnified image of the circled region in the left picture). LPEI, linear polyethylenimine; MCTS, multicellular tumor spheroid; N/P, ratio of the number of amino groups units to a nucleotide unit.

Hypoxia-selective gene expression in the MCTS

To confirm the gene expression in hypoxic cells in the MCTS, we carried out the transfection study using pDNA encoding *Venus* driven by the 5× hypoxia-responsive element (5HRE) promoter (p5HRE + *Venus*). The hypoxia-selectivity of p5HRE + *Venus* was examined in monolayer cultured HuH-7 cells under hypoxic conditions reproduced by iron-chelating agent, deferoxamine mesylate.[20] As shown in Figure 3a, PEG-*b*-P[Asp(DET)] polyplex micelles containing hypoxia-responsive p5HRE + *Venus* showed no gene expression under normoxic conditions (0 μmol/l deferoxamine mesylate) but an appreciable gene expression under hypoxia-mimicking conditions (200 μmol/l deferoxamine mesylate). Note that polyplex micelles containing hypoxia-irresponsive pCAcc + *Venus* exhibited significant gene expression under both normoxic and hypoxic conditions. Thus, p5HRE + *Venus* was demonstrated to be highly selective to hypoxic environments. Then, LPEI and P[Asp(DET)] polyplexes and PEG-*b*-P[Asp(DET)] polyplex micelles containing p5HRE + *Venus* were applied to the transfection to the large-sized MCTS (400–500 μm). As a result, none of 5 spheroids transfected with LPEI polyplexes showed the expression of p5HRE + *Venus* (data not shown), which may be consistent with the expression of pCAcc + *Venus* limited to the periphery of the MCTS (Figure 2b). Surprisingly, P[Asp(DET)] polyplexes exhibited the expression of p5HRE + *Venus* in two of five spheroids at 48 hours after the transfection; however, the gene expression was limited to the outer rims of hypoxic regions at ~100 μm distance from the periphery of the MCTS (Figure 3b; the yellow circle is the initial size of spheroids before the transfection). This result suggests that P[Asp(DET)] polyplexes could penetrate into the inside of the spheroids to some extent. In contrast, PEG-*b*-P[Asp(DET)] polyplex micelles allowed the transfection of p5HRE + *Venus* to a larger number of the cells in the inner region of the MCTS in 7 of 10 spheroids (Figure 3b), suggesting the ability of the polyplex micelles to transfect hypoxic cells inside of the spheroids. To further confirm this effect, two distinct plasmids encoding DsRedC1 (red fluorescence) driven

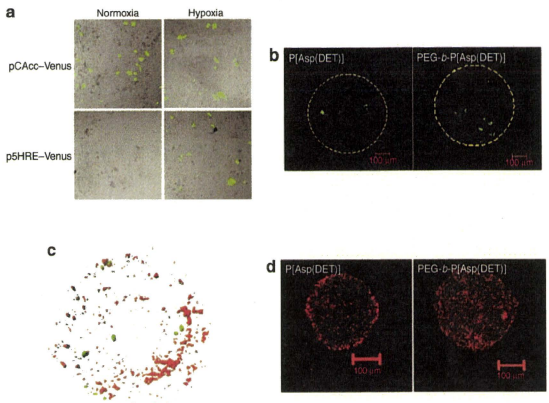

Figure 3 Hypoxia selective gene expression in the MCTS. (**a**) Gene expressions of hypoxia-irresponsive pCAcc + *Venus* and hypoxia-responsive p5HRE + *Venus* in monolayer cultured HuH-7 cells under normoxic and hypoxic conditions. HuH-7 cells were incubated with PEG-*b*-P[Asp(DET)] polyplex micelles (N/P = 20) for 24 hours, followed by additional 24 hours incubation after the medium replacement. Hypoxia-mimicking conditions were reproduced by incubating the cells with iron chelating agent, DFx during the postincubation. (**b**) Gene expressions of hypoxia-responsive p5HRE + *Venus* in the HuH-7 spheroids transfected with P[Asp(DET)] polyplexes and PEG-*b*-P[Asp(DET)] polyplex micelles (N/P = 20). The yellow circle indicates the size of the MCTS at the time of the transfection. (**c**) Piled up images of the gene expressions of hypoxia-irresponsive pCMV-DsRedC1 (red fluorescence) and hypoxia-responsive p5HRE – *Venus* (green fluorescence) in the MCTS transfected with PEG-*b*-P[Asp(DET)] polyplex micelles incorporating each plasmid (N/P = 20). (**d**) Distribution of Cy3-labeled pDNA encapsulated into P[Asp(DET)] polyplexes (N/P = 20) and PEG-*b*-P[Asp(DET)] polyplex micelles (N/P = 20) in HuH-7 MCTS after 24-hour incubation. The images were taken at the center of the spheroids. DFx, deferoxamine mesylate; MCTS, multicellular tumor spheroid; N/P, ratio of the number of amino groups units to a nucleotide unit.

by the cytomegalovirus (CMV) promoter (pCMV-DsRedC1) and *Venus* (green fluorescence) driven by the 5HRE promoter (p5HRE – *Venus*) were independently encapsulated into PEG-*b*-P[Asp(DET)] polyplex micelles, and then applied to the transfection to the MCTS. After 48 hours, optical slices of the MCTS at a depth of 1 μm were taken by confocal microscopy, and then piled up by Imaris software (Carl Zeiss, Jena, Germany) to obtain the three-dimensional localization of each fluorescence. As shown in Figure 3c, the expression of p5HRE – *Venus* was mainly detected in the inner region of the MCTS, whereas the expression of pCMV-DsRedC1 was observed throughout the MCTS. Thus, the hypoxic inner regions of the MCTS were successfully transfected with PEG-*b*-P[Asp(DET)] polyplex micelles.

Percolation of polyplexes and polyplex micelles into the MCTS

The percolation of the polyplexes and polyplex micelles into the MCTS was investigated by using Cy3-labeled pDNA. In this study, the MCTS with a diameter of 200–250 μm was used to detect weak fluorescence from Cy3-labeled pDNA within the spheroids. Figure 3d shows the fluorescent image of Cy3-labeled pDNA at the center of HuH-7 MCTS after 24-hour incubation with polyplexes or polyplex micelles. Note that the treatment of the relatively small-sized MCTS with LPEI polyplexes resulted in destruction of spheroid structures due to the cytotoxicity of LPEI as previously reported.[19] As shown in Figure 3d, P[Asp(DET)] polyplexes displayed apparent fluorescence at the periphery of spheroids. This result is consistent with the previous report that cationic polyplexes could penetrate only the outer 3–5 proliferating cell layers (10–20 μm) of the MCTS.[11] In contrast, the pDNA formulated in PEG-*b*-P[Asp(DET)] polyplex micelles showed well-distributed fluorescence within spheroids, suggesting their percolation into the inside of the spheroids. Similar results were obtained when the MCTS model from a different cell line (*i.e.*, human pancreatic BxPC3 cells) were used (**Supplementary Figure S1**). Thus, polyplex micelles might possess the ability to percolate into the spheroids over cationic polyplexes.

i.t. distribution of polyplexes and polyplex micelles after i.t. injection

The i.t. distribution of naked pDNA, LPEI polyplexes (N/P = 6), P[Asp(DET)] polyplexes (N/P = 20), or PEG-*b*-P[Asp(DET)] polyplex micelles (N/P = 20) after the injection to solid tumors (human pancreatic adenocarcinoma BxPC3 cells) was evaluated by using Cy3-labeled pDNA ($n = 3$). In this experiment, each formulation was coadministered with FluoSphere fluorescent microspheres [particle size: 15 μm, 645 nm/680 nm (Ex/Em)] as a marker for the injection point. The fluorescent images of Cy3-labeled pDNA in BxPC3 tumors are shown in Figure 4a and **Supplementary Figure S2**, and the total pixels of fluorescence area and its localization in the three different regions classified by the distance from the injection point (<100 μm, 100–200 μm, >200 μm) are quantified

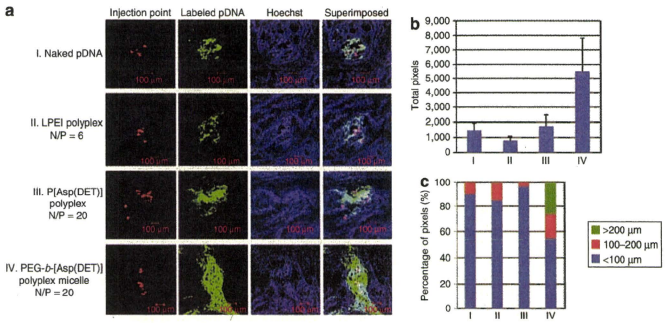

Figure 4 Intratumoral distribution of polyplexes and polyplex micelles after intratumoral injection. (**a**) Distribution of Cy3-labeled pDNA (green fluorescence) in a naked form or encapsulated into LPEI polyplexes (N/P = 6), P[Asp(DET)] polyplexes (N/P = 20), or PEG-*b*-P[Asp(DET)] polyplex micelles (N/P = 20) within human pancreatic adenocarcinoma BxPC3 tumors after intratumoral (i.t.) injection. The red and blue fluorescence are derived from fluorescent beads with a size of 15 μm as an indicator of injection point and Hoechst 33342 for the nuclear staining, respectively (more detailed data are shown in **Supplementary Figure S2**). (**b**) Total pixels and (**c**) percentage of pixels of fluorescent area of Cy3-labeled pDNA in three regions classified by the distance from the injection point. N/P, ratio of the number of amino groups units to a nucleotide unit.

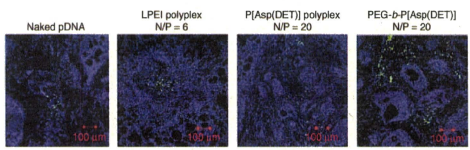

Figure 5 Gene expression of EGFP (green) within BxPC3 tumors at 6 days post-i.t. injection of naked plasmids, LPEI polyplexes (N/P = 6), P[Asp(DET)] polyplexes (N/P = 20), or PEG-b-P[Asp(DET)] polyplex micelles (N/P = 20). The blue fluorescence is derived from Hoechst 33342 for the nuclear staining. EGFP, enhanced green fluorescent protein; LPEI, linear polyethylenimine; N/P, ratio of the number of amino groups units to a nucleotide unit.

in Figure 4b,c, respectively. As a result, PEG-*b*-P[Asp(DET)] polyplex micelles showed a tendency to distribute more widely from the injection point compared with naked pDNA, LPEI and P[Asp(DET)] polyplexes. Note that irregular i.t. distribution of the polyplex micelles may be attributed to the heterogeneous structure of the BxPC3 tumors comprising clusters of dense tumor cells and interstitial tissues as indicated by the nuclear staining with Hoechst 33342.

In vivo gene expression after i.t. injection

The *in vivo* gene expression of fluorescent protein, enhanced green fluorescent protein (EGFP) within the BxPC3 tumors at 6 days post-i.t. injection of naked pDNA, LPEI polyplexes (N/P = 6), P[Asp(DET)] polyplexes (N/P = 20), or PEG-*b*-P[Asp(DET)] polyplex micelles (N/P = 20) was evaluated (n = 3). Note that P[Asp(DET)] polyplexes and polyplex micelles showed the highest transfection at 6 days postincubation in the MCTS models.[19] As shown in Figure 5, PEG-*b*-P[Asp(DET)] polyplex micelles apparently showed a widely distributed expression of EGFP in comparison with naked pDNA, LPEI, and P[Asp(DET)] polyplexes. These results seem to be consistent with the i.t. distribution of polyplex micelles (Figure 4).

Furthermore, the expression of hypoxia-responsive p5HRE + *Venus* within the BxPC3 tumors was evaluated (Figure 6a). The hypoxic region developed far from the vessels in the BxPC3 tumors was confirmed by fluorescein isothiocyanate-conjugated anti-Hypoxyprobe-1 monoclonal antibody (Figure 6b). Similar to Figure 4c, the pixels of fluorescent area in Figure 6a are classified into three different regions and summarized in Figure 6c. As a result, naked pDNA and LPEI polyplexes showed little gene expression, and P[Asp(DET)] polyplexes showed an appreciable gene expression in the region close to the injected point. In contrast, PEG-*b*-P[Asp(DET)] polyplex micelles showed well-distributed gene expression even in the furthest region from the injection point (>200 μm). These results suggest that the polyplex micelles might have the ability to percolate into the tumor tissue, thereby improving the gene transfection in the hypoxic regions of solid tumors.

DISCUSSION

Recently, we compared the transfection ability and cytotoxicity between P[Asp(DET)] polyplexes and PEG-*b*-P[Asp(DET)] polyplex micelles by using MCTS models.[19] We revealed that the PEGylation decreased the cytotoxicity of polyplexes without

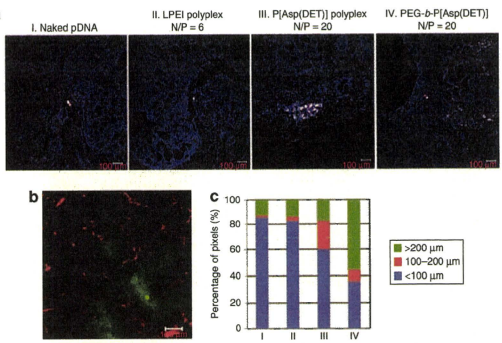

Figure 6 Hypoxia-responsive gene expression after intratumoral injection. (**a**) Gene expression of hypoxia-responsive p5HRE + *Venus* (white) within BxPC3 tumors at 6 days post-i.t. injection of naked plasmids, LPEI polyplexes (N/P = 6), P[Asp(DET)] polyplexes (N/P = 20), or PEG-b-P[Asp(DET)] polyplex micelles (N/P = 20). The red and blue fluorescence are derived from fluorescent beads with a size of 15 μm as an indicator of injection point and Hoechst 33342 for the nuclear staining, respectively. (**b**) Hypoxic regions in BxPC3 solid tumors. The red and green fluorescence are derived from anti-PECAM-1 antibody and anti-Hypoxyprobe-1 antibody, respectively. (**c**) Percentage of pixels of fluorescent area of transfected *Venus* protein in three regions classified by the distance from the injection point. i.t., intratumoral; LPEI, linear polyethylenimine; N/P, ratio of the number of amino groups units to a nucleotide unit.

compromising the transfection efficiency, while delaying the onset of gene expression. In this study, we report another important property of PEG-*b*-P[Asp(DET)] polyplex micelles, *i.e.*, tissue penetrability. We demonstrated that polyplex micelles showed facilitated percolation of loaded pDNA into the tumor tissue in both *in vitro* MCTS models and subcutaneous tumor models. Consequently, polyplex micelles showed a well-distributed gene expression after i.t. injection, allowing the transfection to the hypoxic regions of the tumors. These observations are in good agreement with our previous reports that polymeric micelles incorporating adriamycin showed enhanced percolation into the tumor tissue not only in the MCTS models[16] but also in subcutaneous tumors after intravenous administration.[17] Recently, Mellor *et al.* reported that cationic polyplexes from linear and branched PEI and lipoplexes showed penetration and transfection limited to the outer 3–5 proliferating cell layers in the large-sized MCTS (~474 nm).[11] Consistently, our results (Figures 2b, 3d, and 4–6) also demonstrated not only *in vitro* but also *in vivo* that cationic polyplexes might show the limited penetration and localized transfection within the tumor. Furthermore, the result indicates for the first time that PEGylated polyplexes led loaded pDNA to show improved tissue penetrability compared with cationic polyplexes, exerting the appreciable gene expression in the inner hypoxia region.

PEGylation has apparently an advantage to prevent aggregation of polyplexes in the physiological condition with the presence of considerable amount of salt. Also, the PEGylation effectively masks the cationic nature of the core polyplexes, preventing nonspecific interaction serum proteins and extracellular matrices. Indeed, we observed that the PEG shielding of the P[Asp(DET)] polyplexes decreased the Zeta-potential from +30 mV to +6 mV. Such prevention of aggregate formation and reduced interaction with biological components by PEGylation may contribute to the facilitated percolation of the polyplexes into the tumor tissue. In this regard, the stability of polyplex micelles is an important issue during their penetration process into the tumor tissue. Our previous study revealed that the PEG-*b*-P[Asp(DET)] polyplex micelles showed much higher tolerability against the pDNA exchange reaction with an anionic lipid compared with the P[Asp(DET)] polyplexes.[19] Such increased stability of polyplex micelles is consistent with their improved penetration into the tumor tissue observed here. Furthermore, there are several reports that PEGylated nanoparticles show enhanced passage through the mucosal tissues to overcome intestinal barriers presumably due to the high flexibility and amphiphilicity of PEG chains.[21–23]

The detailed mechanisms of the enhanced percolation of polyplex micelles in the tumor tissue remain to be clarified yet; however, the results in this study clearly demonstrate that polyplex micelles might access the tumor cells in the hypoxic region with the intrinsic functions to deliver therapeutic genes. Thus, polyplex micelles are expected to treat hypoxic regions in the tumor tissue, potentially preventing the recurrence and malignant progression of solid tumors. Together with improved pharmacokinetic parameters, PEGylated polyplexes with a high tissue-percolation property might be promising nonviral vectors for *in vivo* cancer gene therapy.

MATERIALS AND METHODS

Plasmid DNA. The plasmid, pCAcc vector having CAG promoter,[24] was provided by RIKEN Bioresource Center (Ibaraki, Japan). Also, a fragment cDNA of SEYFP-F46L (*Venus*), which is a variant of yellow fluorescent protein with the mutation F46L,[25] was provided by A. Miyawaki at the Brain Science Institute, RIKEN and inserted into the pCAcc vector (pCAcc + *Venus*). Each pDNA was amplified in competent DH5α *Escherichia coli* and purified using HiSpeed Plasmid MaxiKit (Qiagen Sciences, Hilden, Germany). The plasmid, pGL5 vector having p5HRE, was provided by Faculty of Medicine, Kyoto University (Japan).[26] The DNA fragment encoding *Venus* was inserted between *Hind*III and *Xba*I sites of pGL3/5xHRE/CMVmp.

Nonviral vectors. LPEI (ExGen 500, 22 kd) was purchased from Fermentas (Burlington, Ontario, Canada). P[Asp(DET)] and PEG-*b*-P[Asp(DET)] were prepared as previously reported.[12–14] Briefly, β-benzyl-L-aspartate *N*-carboxyanhydride was polymerized by the initiation from the primary amino group of *n*-butylamine and MeO-PEG-NH_2 (M_w: 12,000) to obtain poly(β-benzyl L-aspartate) (PBLA) and PEG-*b*-PBLA, respectively. The degree of polymerization of PBLA was determined to be 98 for PBLA and 101 for PEG-*b*-PBLA by the ^{1}H NMR measurement. Then, PBLA and PEG-*b*-PBLA were reacted with diethylenetriamine (DET) (50 equiv to benzyl group of PBLA segment) under mild anhydrous conditions to obtain P[Asp(DET)] and PEG-*b*-P[Asp(DET)], respectively. The unimodal distribution and the almost 100% conversion of the BLA unit into Asp(DET) unit were confirmed by gel permeation chromatography and ^{1}H NMR measurements.

Preparation of polyplexes. Each polymer was mixed with pDNA in 10 mmol/l Tris–HCl (pH 7.4) at varying N/P ratios (final pDNA concentration: 100 μg/ml). Polyplex was applied to each well for transfection 30 minutes after preparation. Polyplex micelle was applied to each well for transfection after overnight incubation at ambient temperature.

Cell culture and preparation of MCTS. Human hepatoma HuH-7 cells (from JCRB Cell Bank, Osaka, Japan) and human pancreatic adenocarcinoma BxPC3 cells (from ATCC, Manassas, VA) were maintained in Dulbecco's modified Eagle's medium and RPMI 1640 medium, respectively, supplemented with 10% fetal bovine serum in a humidified atmosphere containing 5% CO_2 at 37 °C. MCTS were prepared by using the plate designed for spheroid formation (Sumiloncelltight; Sumitomo Bakelite, Tokyo, Japan) as reported previously.[15,18] The size of MCTS can be controlled by the incubation period. During the incubation, the medium was replaced by fresh medium containing 10% fetal bovine serum every 3 days.

Live/dead assay. Live and dead assay was accomplished with the Live/Dead kit protocol (Molecular Probes, Carlsbad, CA). MCTS was rinsed with PBS(–) and then incubated with a solution containing 0.8 μmol/l calcein AM [495 nm/515 nm (Ex/Em)] and 4 μmol/l EthD-1 (495 nm/635 nm) in PBS(–) for 3 hours at 37 °C, followed by the observation by LSM 510 confocal laser scanning microscope (CLSM) (Carl Zeiss).

Transfection to MCTS. MCTS was incubated for 6–8 days until the diameter became >400–500 μm. Then, each polyplex solution containing 1 μg pDNA was applied to each well for the transfection. After 24-hour incubation, the medium was replaced by fresh medium, followed by additional 24-hour incubation. The gene expression of the *Venus* or EGFP was then evaluated through the observation by CLSM.

Percolation of nonviral vectors into the MCTS. To visualize the distribution of nonviral vectors in MCTS, pDNA was labeled with Label IT Cy3 Labeling Kit (Mirus, Piscataway, NJ). In this experiment, MCTS with the diameter of 200–250 μm was incubated with polyplexes or polyplex micelles containing 1 μg Cy3-labeled pDNA for 24 hours. After 24-hour incubation, MCTS was harvested and rinsed, followed by observation by CLSM.

Animal models. BALB/c nude mice (female, 5 weeks old) were obtained from Charles River Laboratories (Tokyo, Japan). BxPC3 cells (5×10^6 cells in 100 μl of PBS) were injected subcutaneously into the BALB/c nude mice and allowed to grow for 2–3 weeks to reach the proliferative phase. All animal experimental protocols were performed in accordance with the policies of the Animal Ethics Committee of the University of Tokyo.

Percolation of nonviral vectors in solid tumors. After the tumor size reached 6–8 mm in a diameter, the mice received the i.t. injection of 2 μg Cy3-labeled pDNA in a naked or polyplex-encapsulated form [20 μl in 10 mmol/l HEPES buffer (pH 7.4)] by using the Hamilton Microliter Syringe (Hamilton, Reno, NV). In this experiment, 5 μl of FluoSpheres fluorescent microspheres (particle size: 15 μm, 645 nm/680 nm) were mixed with Cy3-labeled pDNA solution and simultaneously injected into the BxPC3 tumor for indication of the injection point. After 24 hours, the tumors were excised and fixed with 10% formalin and sucrose PBS(–), followed by freezing in dry-iced acetone. Frozen samples were sectioned at 10-μm thickness in a cryostat, and stained with Hoechst 33342 (Dojindo Laboratories, Tokyo, Japan). The fluorescent images were then observed by CLSM.

Transfection to solid tumors. According to the protocols for the percolation study, the tumor-bearing mice received the i.t. injection of 2 μg pCAcc + EGFP or p5HRE + *Venus* in a naked or polyplex-encapsulated form. The animals administered with pCAcc + EGFP were killed at 6 days postinjection, and the excised tumors were fixed as previously described. The fluorescence of frozen section of solid tumors was observed by CLSM. On the other hand, the animals administered with p5HRE + *Venus* were administered with Hypoxyprobe-1 (Millipore Chemicon, Billerica, MA) at 60 mg/kg via tail vein at 6 days postinjection, and then killed for removal of solid tumors. Frozen sections of the xenograft were stained with rat anti-PECAM-1 antibody (BD Pharmingen, Franklin Lakes, NJ), and subsequently stained with Alexa 594-conjugated anti-rat IgG antibody (Invitrogen Molecular Probes, Carlsbad, CA) and fluorescein isothiocyanate-conjugated anti-Hypoxyprobe-1 MAb. The section was further counter-stained with TOTO-3 (Invitrogen Molecular Probes), and the fluorescence images were captured by CLSM.

Quantitative analysis of fluorescent images. The pixels of fluorescent area of Cy3-labeled pDNA or transfected *Venus* protein in the tumor section were quantified by using the Image J software (http://rsb.info.nih.gov/ij/), and classified into three different regions by the distance from the injection point (<100 μm, 100–200 μm, >200 μm).

SUPPLEMENTARY MATERIAL

Figure S1. Distribution of labeled pDNA in BxPC3 MCTS transfected by each polyplex or polyplex micelles in intersectional profiles at the shown slices (Optical slice at the center of MCTS. Red fluorescence is Cy3 labeled-pDNA).

Figure S2. Distribution of Cy3-labeled pDNA (green fluorescence) in a naked form or encapsulated into LPEI polyplexes (N/P=6), P[Asp(DET)] polyplexes (N/P=20) or PEG-*b*-P[Asp(DET)] polyplex micelles (N/P=20) within human pancreatic adenocarcinoma BxPC3 tumors after the intratumoral injection.

ACKNOWLEDGMENTS

We thank Kotoe Date (the University of Tokyo) for technical assistance. This work was supported in part by the Core Research Program for Evolutional Science and Technology from Japan Science and Technology Agency.

REFERENCES

1. Boussif, O, Lezoualc'h, F, Zanta, MA, Mergny, MD, Scherman, D, Demeneix, B *et al.* (1995). A versatile vector for gene and oligonucleotide transfer into cells in culture and *in vivo*: polyethylenimine. *Proc Natl Acad Sci USA* **92**: 7297–7301.
2. Ogris, M and Wagner, E (2002). Targeting tumors with non-viral gene delivery systems. *Drug Discov Today* **7**: 479–485.
3. Merdan, T, Kopecek, J and Kissel, T (2002). Prospects for cationic polymers in gene and oligonucleotide therapy against cancer. *Adv Drug Deliv Rev* **54**: 715–758.
4. Pack, DW, Hoffman, AS, Pun, S and Stayton, PS (2005). Design and development of polymers for gene delivery. *Nat Rev Drug Discov* **4**: 581–593.
5. Erbacher, P, Roche, AC, Monsigny, M and Midoux, P (1995). Glycosylated polylysine/DNA complexes: gene transfer efficiency in relation with the size and the sugar substitution level of glycosylated polylysines and with the plasmid size. *Bioconjug Chem* **6**: 401–410.
6. Merdan, T, Callahan, J, Petersen, H, Kunath, K, Bakowsky, U, Kopecková, P *et al.* (2003). Pegylated polyethylenimine-Fab' antibody fragment conjugates for targeted gene delivery to human ovarian carcinoma cells. *Bioconjug Chem* **14**: 989–996.
7. Ogris, M, Brunner, S, Schüller, S, Kirchels, R and Wagner, E (1999). PEGylated DNA/transferrin-PEI complexes: reduced interaction with blood components, extended circulation in blood and potential for systemic gene delivery. *Gene Ther* **6**: 595–605.

8. Harada-Shiba, M, Yamauchi, K, Harada, A, Takamisawa, I, Shimokado, K and Kataoka, K (2002). Polyion complex micelles as vectors in gene therapy—pharmacokinetics and *in vivo* gene transfer. *Gene Ther* **9**: 407–414.
9. Jain, RK (2001). Delivery of molecular and cellular medicine to solid tumors. *Adv Drug Deliv Rev* **46**: 149–168.
10. Minchinton, AI and Tannock, IF (2006). Drug penetration in solid tumours. *Nat Rev Cancer* **6**: 583–592.
11. Mellor, HR, Davies, LA, Caspar, H, Pringle, CR, Hyde, SC, Gill, DR *et al.* (2006). Optimising non-viral gene delivery in a tumour spheroid model. *J Gene Med* **8**: 1160–1170.
12. Kanayama, N, Fukushima, S, Nishiyama, N, Itaka, K, Jang, WD, Miyata, K *et al.* (2006). A PEG-based biocompatible block catiomer with high buffering capacity for the construction of polyplex micelles showing efficient gene transfer toward primary cells. *ChemMedChem* **1**: 439–444.
13. Miyata, K, Oba, M, Nakanishi, M, Fukushima, S, Yamasaki, Y, Koyama, H *et al.* (2008). Polyplexes from poly(aspartamide) bearing 1,2-diaminoethane side chains induce pH-selective, endosomal membrane destabilization with amplified transfection and negligible cytotoxicity. *J Am Chem Soc* **130**: 16287–16294.
14. Akagi, D, Oba, M, Koyama, H, Nishiyama, N, Fukushima, S, Miyata, T *et al.* (2007). Biocompatible micellar nanovectors achieve efficient gene transfer to vascular lesions without cytotoxicity and thrombus formation. *Gene Ther* **14**: 1029–1038.
15. Itaka, K, Ohba, S, Miyata, K, Kawaguchi, H, Nakamura, K, Takato, T *et al.* (2007). Bone regeneration by regulated *in vivo* gene transfer using biocompatible polyplex nanomicelles. *Mol Ther* **15**: 1655–1662.
16. Bae, Y, Nishiyama, N, Fukushima, S, Koyama, H, Yasuhiro, M and Kataoka, K (2005). Preparation and biological characterization of polymeric micelle drug carriers with intracellular pH-triggered drug release property: tumor permeability, controlled subcellular drug distribution, and enhanced *in vivo* antitumor efficacy. *Bioconjug Chem* **16**: 122–130.
17. Kano, MR, Bae, Y, Iwata, C, Morishita, Y, Yashiro, M, Oka, M *et al.* (2007). Improvement of cancer-targeting therapy, using nanocarriers for intractable solid tumors by inhibition of TGF-beta signaling. *Proc Natl Acad Sci USA* **104**: 3460–3465.
18. Sutherland, RM (1988). Cell and environment interactions in tumor microregions: the multicell spheroid model. *Science* **240**: 177–184.
19. Han, M, Bae, Y, Nishiyama, N, Miyata, K, Oba, M and Kataoka, K (2007). Transfection study using multicellular tumor spheroids for screening non-viral polymeric gene vectors with low cytotoxicity and high transfection efficiencies. *J Control Release* **121**: 38–48.
20. An, WG, Kanekal, M, Simon, MC, Maltepe, E, Blagosklonny, MV and Neckers, LM (1998). Stabilization of wild-type p53 by hypoxia-inducible factor 1alpha. *Nature* **392**: 405–408.
21. Huang, Y, Leobandung, W, Foss, A and Peppas, NA (2000). Molecular aspects of muco- and bioadhesion: tethered structures and site-specific surfaces. *J Control Release* **65**: 63–71.
22. Samuel, KL, Elizabeth, OD, Harrold, S, Man, ST, Wang, Y, Cone, R *et al.* (2007). Rapid transport of large polymeric nanoparticles in fresh undiluted human mucus. *Proc Natl Acad Sci USA* **104**: 1482–1487.
23. Yoncheva, K, Guembe, L, Campanero, MA and Irache, JM (2007). Evaluation of bioadhesive potential and intestinal transport of pegylated poly(anhydride) nanoparticles. *Int J Pharm* **334**: 156–165.
24. Niwa, H, Yamamura, K and Miyazaki, J (1991). Efficient selection for high-expression transfectants with a novel eukaryotic vector. *Gene* **108**: 193–199.
25. Nagai, T, Ibata, K, Park, ES, Kubota, M, Mikoshiba, K and Miyawaki, A (2002). A variant of yellow fluorescent protein with fast and efficient maturation for cell-biological applications. *Nat Biotechnol* **20**: 87–90.
26. Harada, H, Kizaka-Kondoh, S and Hiraoka, M (2005). Optical imaging of tumor hypoxia and evaluation of efficacy of a hypoxia-targeting drug in living animals. *Mol Imaging* **4**: 182–193.

Protein Delivery

DOI: 10.1002/anie.200900064

Charge-Conversional Polyionic Complex Micelles—Efficient Nanocarriers for Protein Delivery into Cytoplasm**

*Yan Lee, Takehiko Ishii, Horacio Cabral, Hyun Jin Kim, Ji-Hun Seo, Nobuhiro Nishiyama, Hiroki Oshima, Kensuke Osada, and Kazunori Kataoka**

In the postgenomic era, the elucidation of protein function is one of the most important challenges in biological fields as the development of protein-based therapeutics has great potential in medicinal science. Enhancement and knockout of a specific protein expression are among the various methods that have been used for fundamental research into protein function. The direct delivery of proteins into cells is probably one of the simplest and most decisive ways to examine protein function, as no interference or artifacts occur during the transcription–translation pathway. Moreover, an efficient in vivo protein delivery is essential for therapeutic applications. Although various protein-based biopharmaceuticals have been developed, the instability of proteins in serum and the lack of a delivery method into cytoplasm has limited further success.[1] Many research groups have therefore concentrated on the development of protein delivery methods[2] such as hydrogels, liposomes, nanotubes, or inorganic carriers, but a highly efficient delivery method that offers serum stability and generality has not yet been developed.

We report herein a novel approach for protein delivery based on polyionic complex (PIC) micelles, which are well-defined core–shell supramolecular structures formed through electrostatic interactions when diblock copolymers with both a neutral and an ionic block mix with their counterions.[3] Because the shell of the neutral block protects the core from external deactivation pathways such as enzymatic attack or aggregation, the PIC micelle can act as a molecular container. PIC micelles have also been used as delivery carriers for drugs or biomacromolecules because of their high stability, reduced immune response, and elongated circulation time, which arise from their biocompatible surfaces and high molecular weights.[4] We have successfully developed PIC micelles, which contain a block copolymer with poly(ethylene glycol) (PEG) as a neutral block and a poly(amino acid) as an ionic block,[5] for DNA and RNA delivery. However, the protein-containing PIC micelles dissociated immediately at a physiological salt concentrations, which has limited their biological application.[6] Stabilized PIC micelles could be obtained by cross-linking with glutaraldehyde; it was difficult to apply these micelles in the human body because of the toxicity of glutaraldehyde and the irreversibility of the cross-linking.[7] The salt stability of the PIC micelles is closely related to the charge density of its components. For example, PIC micelles of DNA with high charge density (−308 Da per charge) were stable, but those with lysozyme (+1980 Da per charge) dissociated rapidly at the physiological salt concentration.

Therefore, in order to obtain a higher micelle stability, we attempted to increase the charge density of the protein by employing a reversible conjugation. Citraconic amide and *cis*-aconitic amide, derivatives of the maleic acid amide, are stable at the normal physiological pH value of 7.4, but degrade at the endosomal pH value of 5.5 to expose primary amines, with a charge conversion from negative to positive.[8] If a protein has a sufficient amount of lysine groups that can be modified to citraconic amides or *cis*-aconitic amides, the pI (isoelectric point) of the protein decreases significantly. Moreover, because the *cis*-aconitic amide exposes two carboxylate groups per reacted amine group, the anionic charge density could be reversibly increased (Scheme 1). We expected that the PIC micelles that contain the modified protein would have an increased salt stability because of the high charge density, and that they could release the original protein after charge conversion in the endosome.

We selected equine heart cytochrome c (CytC; M_w = 12384 Da), an essential protein in the electron transfer of the mitochondria, as a model protein. The CytC is a cationic protein with a charge density of + 1391 Da per charge, which arises from the presence of three aspartate, nine glutamate, two arginine, and 19 lysine units. However, CytC could not form the PIC micelles with poly(ethylene glycol)–poly[(*N*'-succinyl-2-aminoethyl(aspartamide)] (PEG–pAsp(EDA-Suc); **2**), an anionic block copolymer, in the presence of NaCl (150 mM). We modified CytC with citraconic anhydride and *cis*-aconitic anhydride to increase the charge density (the synthetic procedure for all block copolymers and the CytC modification method are described in detail in the Supporting Information). The resulting anionic proteins were Cyt–Cit (−501 Da per charge) and Cyt–Aco (−320 Da per charge).

[*] Dr. Y. Lee, Dr. H. Cabral, Dr. N. Nishiyama, Prof. Dr. K. Kataoka
Center for Disease Biology and Integrative Medicine
Graduate School of Medicine, The University of Tokyo
7-3-1 Hongo, Bunkyo-ku, Tokyo 113-0033 (Japan)
Fax: (+81) 3-5841-7139
E-mail: kataoka@bmw.t.u-tokyo.ac.jp
Dr. T. Ishii, Prof. Dr. K. Kataoka
Department of Bioengineering, The University of Tokyo
7-3-1 Hongo, Bunkyo-ku, Tokyo 113-8656 (Japan)
H. J. Kim, J. Seo, H. Oshima, Dr. K. Osada, Prof. Dr. K. Kataoka
Department of Materials Engineering, The University of Tokyo
7-3-1 Hongo, Bunkyo-ku, Tokyo 113-8656 (Japan)
Dr. N. Nishiyama, Prof. Dr. K. Kataoka
Center for Nanobio Integration, The University of Tokyo
7-3-1 Hongo, Bunkyo-ku, Tokyo 113-8656 (Japan)

[**] This work was supported by a Core Research for Evolutional Science and Technology (CREST) grant from the Japan Science and Technology Agency (JST).

Supporting information for this article is available on the WWW under http://dx.doi.org/10.1002/anie.200900064.

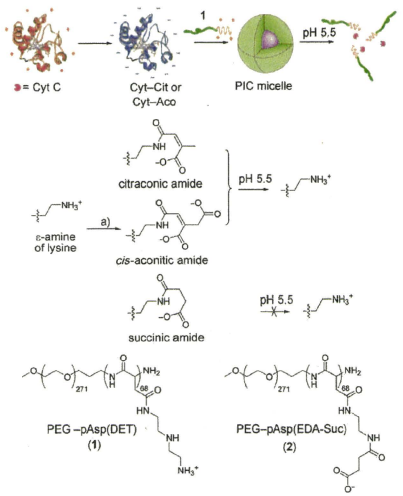

Scheme 1. Schematic representation showing the preparation of the charge-conversional PIC micelles containing CytC derivatives and PEG–pAsp(DET). a) Citraconic anhydride (or *cis*-aconitic anhydride/succinic anhydride).

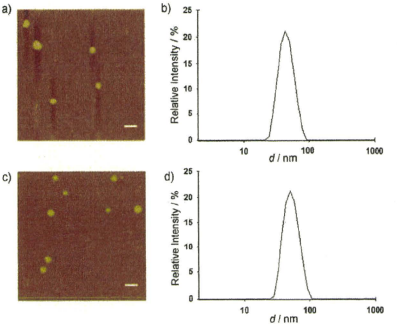

Figure 1. AFM images of the PIC micelles containing a) Cyt–Cit and c) Cyt–Aco. DLS distributions of the PIC micelles containing b) Cyt–Cit and d) Cyt–Aco (N/C ratio = 2). Scale bars: 200 nm.

The formation of the PIC micelle containing the modified CytC and a block copolymer, PEG–poly[*N*-{*N'*-(2-aminoethyl)-2-aminoethyl}aspartamide] (PEG–pAsp(DET); **1**), was examined because PEG–pAsp(DET) has been reported to efficiently deliver DNA into cytoplasm and to have minimal toxicity.[9] The pH-sensitive endosome-destabilization activity of the pAsp(DET) block was shown to be the main reason for the high delivery efficiency.[10] Dynamic light scattering (DLS) measurements showed the PIC micelles to have a unimodal size distribution with diameters of about 50 nm and PDI values of about 0.05, even at physiological salt concentration (150 mM NaCl; Table 1). The spherical shape of the micelles was confirmed by using AFM (Figure 1). The spherical PIC micelles were formed at the N/C (amine/carboxylate) ratio of 2. Considering that one *N'*-(2-aminoethyl)-2-aminoethyl group has one positive charge at pH 7.4[11] because of the pKa difference between two amines, the PIC micelles could be formed at the charge ratio (+/−) of 1. Consequently, we succeeded in forming stable and stoichiometric PIC micelles under physiological salt conditions, by increasing the charge density of the protein without cross-linking.

Table 1: The formation of the PIC micelles between the block copolymer and CytC derivatives.

Protein	Charge density [Da per charge][a]	pI[a]	Diameter [nm][b]	PDI[b]
CytC[c]	+1391	9.57	n.d.	n.d.
Cyt–Cit[d]	−501	3.71	43.3	0.046
Cyt–Aco[d]	−320	3.47	50.1	0.055

[a] The calculation is described in the Supporting Information. [b] Determined by using DLS. [c] Compound **2** was used as the anionic block copolymer. [d] Compound **1** was used as the cationic block copolymer.

The resulting citraconic amide and *cis*-aconitic amide in Cyt–Cit and Cyt–Aco showed rapid degradability at pH 5.5 (see Figure S1 in the Supporting Information). At pH 5.5, about 80% of the modified lysine reverted to the original lysine within 2 hours, whereas at pH 7.4, only 20–30% reverted, even after 24 hours. As the degradation took place concurrently with the charge conversion from negative to positive, the corresponding dissociation of the PIC micelles was expected to occur. The dissociation was analyzed by using the fluorescence quenching–dequenching method.[12] The fluorescence intensity of the Alexa Fluor 488 labeled CytC derivatives in the core of the PIC micelles was reduced significantly because of the probe–probe quenching effect (<20%). However, the protein release from the PIC micelles induced the recovery of the fluorescence intensity (Figure 2). Over 50% of Cyt–Cit was released from the PIC micelles within 4 hours at pH 5.5, whereas only 10% was released even after 8 hours at pH 7.4. Experiments with Cyt–Aco showed similar release profiles but with a slower rate, which is probably because Cyt–Aco has a higher charge density than Cyt–Cit. The bioactivity of the released CytC from the PIC micelles was also analyzed with a 2,2'-azino-bis(3-ethylbenzthiazoline-6-sulfonic acid) (ABTS) assay (see Figure S4 in the Supporting Information).[13] No difference was observed between the released CytC and the native CytC, which means that the modification–reversion cycle does not affect the activity of CytC. Because the only modification was the change of the amino acids from hydrophilic (+) to hydrophilic (−), extreme conformational denaturation that affected the protein activity was probably limited.

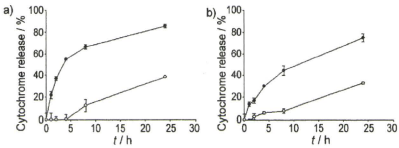

Figure 2. Release of the CytC derivatives from the PIC micelles containing a) Cyt–Cit and b) Cyt–Aco at 37 °C at pH 5.5 (●) and pH 7.4 (○). Each error bar represents the standard deviation of three experiments.

Finally, the delivery efficiency of the charge-conversional PIC micelles on a human hepatoma cell line (HuH-7) was examined. The intracellular distribution of the CytC derivatives labeled with Alexa Fluor 488 (green) was investigated by using confocal laser scanning microscopy (CLSM). The cell images after incubation for 24 h are shown in Figure 3. Because the late endosome and lysosome were stained by LysoTracker Red (red), the CytC in the endosome was detected as yellow. The yellow fluorescence turned to green after protein release from the endosome (see Figure S5 in the Supporting Information for the quantification of the green and red fluorescence colocalization). The native CytC and succinyl CytC (Cyt–Suc), the non-charge-conversional anionic derivative, were used as the controls. As shown in Figure 3a, almost no green fluorescence was detected when the cells were incubated with the native CytC. The lack of green fluorescence was expected, because it is difficult for hydrophilic proteins to penetrate through the plasma membrane. The cells incubated by the PIC micelles containing Cyt–Suc and the polymer **1** showed approximately yellow fluorescence (colocalization ratio (CR) = 0.803); Figure 3b), which means that significant cellular uptake but no endosomal escape occurred. Because the PIC micelles containing Cyt–Suc and **1** did not show any dissociation, even after 24 h at pH 5.5 (see Figure S3 in the Supporting Information), the low efficiency of the endosomal escape is quite reasonable when it is considered that direct contact between the cationic (pAsp(DET)) block and endosomal membrane is important for endosomal escape to occur.[14]

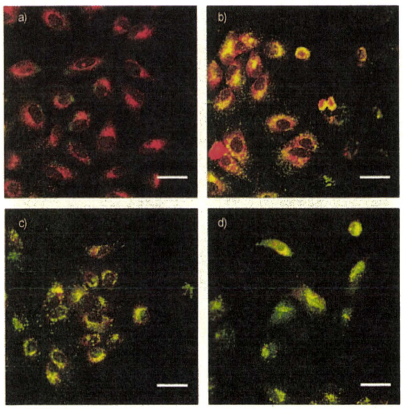

Figure 3. CLSM images of HuH-7 delivered by a) free native CytC, b) Cyt–Suc PIC, c) Cyt–Aco PIC, and d) Cyt–Cit PIC micelles after 24 h transfection. Each CytC derivative was labeled with Alexa Fluor 488 (green). The late endosome and lysosome were stained with LysoTracker Red (red). Scale bars: 50 μm.

In contrast, the charge-conversional PIC micelles containing Cyt–Aco or Cyt–Cit showed strong green fluorescence as well as yellow fluorescence (Figure 3c,d). It was assumed that the polymer **1** released from the PIC micelle could come into direct contact with the endosomal membrane to induce the efficient escape of the CytC. When the two charge-conversional PIC micelles are compared, micelles containing Cyt–Cit (CR = 0.498) showed more efficient endosomal release and resulting cytosolic distribution than Cyt–Aco (CR = 0.682). This result is probably due to the higher sensitivity of Cyt–Cit to the pH reduction over Cyt–Aco. The faster dissociation of the Cyt–Cit micelles in the endosome could lead to faster endosomal escape and diffusion into the cytoplasm.

In summary, we have developed an efficient method, which is based on charge-conversional PIC micelles, of protein delivery into cytoplasm. The stability of the PIC micelle under physiological salt conditions was significantly improved by increasing the charge density of the protein without any cross-linking. The charge conversion of the protein induced the efficient endosomal release, especially in the case of the PIC micelles containing Cyt–Cit. The long circulation time of the PIC micelles and controlled release activity of the charge-conversional moiety were combined in our charge-conversional PIC micelles, which could make them highly valuable for in vivo protein delivery. Moreover, when considering that the molecular weight of the PIC micelles is well over several megadaltons, these charge-conversional PIC micelles could potentially be optimal for the intracellular delivery of high-molecular-weight membrane-impermeable proteins.

Received: January 6, 2009
Published online: March 17, 2009

Keywords: charge conversion · cytochromes · drug delivery · endosomes · micelles

[1] I. M. Tomlinson, *Nat. Biotechnol.* **2004**, *22*, 521–522.
[2] a) K. Y. Lee, S. H. Yuk, *Prog. Polym. Sci.* **2007**, *32*, 669–697; b) N. W. S. Kam, Z. Liu, H. Dai, *Angew. Chem.* **2006**, *118*, 591–595; *Angew. Chem. Int. Ed.* **2006**, *45*, 577–581; c) I. I. Slowing, B. G. Trewyn, V. S. Y. Lin, *J. Am. Chem. Soc.* **2007**, *129*, 8845–8849.
[3] a) A. Harada, K. Kataoka, *Macromolecules* **1995**, *28*, 5294–5299; b) A. V. Kabanov, T. K. Bronich, V. A. Kabanov, K. Yu, A. Eisenberg, *Macromolecules* **1996**, *29*, 6797–6802; c) M. A.

Cohen Stuart, N. A. M. Besseling, R. G. Fokkink, *Langmuir* **1998**, *14*, 6846–6849.
[4] a) G. S. Kwon, K. Kataoka, *Adv. Drug Delivery Rev.* **1995**, *16*, 295–309; b) K. Kataoka, A. Harada, Y. Nagasaki, *Adv. Drug Delivery Rev.* **2001**, *47*, 113–131; c) M. Harada-Shiba, K. Yamauchi, A. Harada, I. Takamisawa, K. Shimokado, K. Kataoka, *Gene Ther.* **2002**, *9*, 407–414.
[5] a) K. Kataoka, H. Togawa, A. Harada, K. Yasugi, T. Matsumoto, S. Katayose, *Macromolecules* **1996**, *29*, 8556–8557; b) S. Katayose, K. Kataoka, *Bioconjugate Chem.* **1997**, *8*, 702–707; c) K. Itaka, N. Kanayama, N. Nishiyama, W. D. Jang, Y. Yamasaki, K. Nakamura, H. Kawaguchi, K. Kataoka, *J. Am. Chem. Soc.* **2004**, *126*, 13612–13613.
[6] a) A. Harada, K. Kataoka, *Macromolecules* **1998**, *31*, 288–294; b) A. Harada, K. Kataoka, *J. Am. Chem. Soc.* **1999**, *121*, 9241–9242; c) M. Jaturanpinyo, A. Harada, X. Yuan, K. Kataoka, *Bioconjugate Chem.* **2004**, *15*, 344–348.
[7] X. Yuan, Y. Yamasaki, A. Harada, K. Kataoka, *Polymer* **2005**, *46*, 7749–7758.
[8] a) J. K. Shetty, J. E. Kinsella, *Biochem. J.* **1980**, *191*, 269–272; b) Y. Lee, S. Fukushima, Y. Bae, S. Hiki, T. Ishii, K. Kataoka, *J. Am. Chem. Soc.* **2007**, *129*, 5362–5363; c) Y. Lee, K. Miyata, M. Oba, T. Ishii, S. Fukushima, M. Han, H. Koyama, N. Nishiyama, K. Kataoka, *Angew. Chem.* **2008**, *120*, 5241–5244; *Angew. Chem. Int. Ed.* **2008**, *47*, 5163–5166.
[9] N. Kanayama, S. Fukushima, N. Nishiyama, K. Itaka, W-D. Jang, K. Miyata, Y. Yamasaki, U-I. Chung, K. Kataoka, *ChemMedChem* **2006**, *1*, 439–444.
[10] K. Miyata, M. Oba, M. Nakanishi, S. Fukushima, Y. Yamasaki, H. Koyama, N. Nishiyama, K. Kataoka, *J. Am. Chem. Soc.* **2008**, *130*, 16287–16294.
[11] K. Masago, K. Itaka, N. Nishiyama, U. Chung, K. Kataoka, *Biomaterials* **2007**, *28*, 5169–5175.
[12] a) S. Kwon, J. H. Carson, *Anal. Biochem.* **1998**, *264*, 133–140; b) Y. Lee, H. Mo, H. Koo, J. Y. Park, M. Y. Cho, G. Jin, J. S. Park, *Bioconjugate Chem.* **2007**, *18*, 13–18; c) B. Z. Packard, A. Komoriya, D. D. Toptygin, L. Brand, *J. Phys. Chem. B* **1997**, *101*, 5070–5074.
[13] R. E. Childs, W. G. Bardsley, *Biochem. J.* **1975**, *145*, 93–103.
[14] S. Takae, K. Miyata, M. Oba, T. Ishii, N. Nishiyama, K. Itaka, Y. Yamasaki, H. Koyama, K. Kataoka, *J. Am. Chem. Soc.* **2008**, *130*, 6001–6009.

Environment-Responsive Block Copolymer Micelles with a Disulfide Cross-Linked Core for Enhanced siRNA Delivery

Satoru Matsumoto,[†] R. James Christie,[†] Nobuhiro Nishiyama,[§,⊥] Kanjiro Miyata,[‡,⊥] Atsushi Ishii,[†,#] Makoto Oba,[∥] Hiroyuki Koyama,[∥] Yuichi Yamasaki,[†,⊥] and Kazunori Kataoka*[,†,‡,§,⊥,▽]

Departments of Materials Engineering and Bioengineering, Graduate School of Engineering, Center for Disease Biology and Integrative Medicine and Department of Clinical Vascular Regeneration, Graduate School of Medicine, and Center for NanoBio Integration, The University of Tokyo, 7-3-1 Hongo, Bunkyo-ku, Tokyo, Japan, NanoCarrier Co., Ltd., 5-4-19 Kashiwanoha, Kashiwa, Chiba 277-0882, Japan, and CREST, Japan Science and Technology Agency, Japan

Received September 4, 2008; Revised Manuscript Received November 5, 2008

A core−shell-type polyion complex (PIC) micelle with a disulfide cross-linked core was prepared through the assembly of iminothiolane-modified poly(ethylene glycol)-*block*-poly(L-lysine) [PEG-*b*-(PLL-IM)] and siRNA at a characteristic optimum mixing ratio. The PIC micelles showed a spherical shape of ~60 nm in diameter with a narrow distribution. The micellar structure was maintained at physiological ionic strength but was disrupted under reductive conditions because of the cleavage of disulfide cross-links, which is desirable for siRNA release in the intracellular reductive environment. Importantly, environment-responsive PIC micelles achieved 100-fold higher siRNA transfection efficacy compared with non-cross-linked PICs prepared from PEG-*b*-poly(L-lysine), which were not stable at physiological ionic strength. PICs formed with PEG-*b*-(PLL-IM) at nonoptimum ratios did not assemble into micellar structure and did not achieve gene silencing following siRNA transfection. These findings show the feasibility of core cross-linked PIC micelles as carriers for therapeutic siRNA and show that stable micellar structure is critical for effective siRNA delivery into target cells.

Introduction

siRNA is a 19−21 base-paired double-stranded RNA that plays a key role in the post-transcriptional gene silencing phenomenon called RNA interference, or RNAi.[1,2] Because siRNAs induce highly efficient gene silencing at the translation level, many efforts have been undertaken to transform their use from a research tool to a therapeutic agent.[3] A reason for the excitement of RNAi therapies is that the therapeutic target (mRNA) resides in the cell cytoplasm, and thus the nuclear membrane is not an obstacle as in DNA-based therapies. Some studies have already progressed to clinical trials, but almost all cases utilize local administration, an application limited to readily accessible tissues such as those found in the ocular and respiratory systems.[4] Despite great promises of therapeutic potential, many obstacles currently prevent systemic application of siRNA. For example, siRNAs are known to degrade rapidly into noneffective fragments in the RNase-rich physiological environment. Additionally, systemically administered naked siRNAs are rapidly eliminated from circulation, with plasma half lives reported to be as short as 0.03 h in mice[5] and 0.1 h in rats.[6] It is clear that an innovative carrier system for systemic administration is required for further development of siRNA as a universal drug. Fundamental design and evaluation of an siRNA carrier, which could be developed into a system for therapeutic use, was the specific aim of this work.

Recently, a number of polyion complexes (PICs) formed through electrostatic interaction between anionic siRNA and cationic polymers have been investigated as carriers of therapeutic siRNA. For example, polyethylenimine (PEI) is a well known cationic polymer that is capable of transfecting nucleic acids.[7] However, the majority of intravenously administered PEI/nucleic acid complexes seem to undergo entrapment by pulmonary capillary beds, resulting in rapid clearance from circulation.[8,9] Modification of PEI with poly(ethylene glycol) (PEG),[10,11] targeting ligand, or both was examined as a method for improving the pharmacokinetics (PK) of PICs because PEGylation of drug carriers generally prolongs blood circulation time and certain ligands direct carriers to target tissues. Although the ligand-installed PEGylated PEI/siRNA complex demonstrated remarkable antitumor effects, no significant extension in the circulation time of siRNA in the blood stream was observed, and eventually, a considerable amount of the injected PIC was unfavorably distributed to nontarget organs such as the liver, lungs, and spleen.[11] Alternatively, PEGylated PICs have been prepared through electrostatic interaction between PEG-*block*-polycation copolymers and nucleic acids such as plasmid DNA or antisense oligo-DNA and are termed PIC micelles because of a core−shell structure with the core surrounded by a dense PEG corona.[12,13] These PIC micelles demonstrate remarkable properties as delivery vehicles for DNA: excellent colloidal stability in proteinaceous media, protection of incorporated DNA against enzymatic degradation, and prolonged blood circulation.[14,15] Hence, PIC micelles have been

* Corresponding author. Tel: +81-3-5841-7138. Fax: +81-3-5841-7139. E-mail: kataoka@bmw.t.u-tokyo.ac.jp.
[†] Department of Materials Engineering, Graduate School of Engineering, The University of Tokyo.
[‡] Department of Bioengineering, Graduate School of Engineering, The University of Tokyo.
[§] Center for Disease Biology and Integrative Medicine, Graduate School of Medicine, The University of Tokyo.
[∥] Department of Clinical Vascular Regeneration, Graduate School of Medicine, The University of Tokyo.
[⊥] Center for NanoBio Integration, The University of Tokyo.
[#] NanoCarrier Co., Ltd.
[▽] Japan Science and Technology Agency.

10.1021/bm800985e CCC: $40.75
Published on Web 12/05/2008

considered to be siRNA carriers,[16] but little is known, particularly from a physicochemical viewpoint, about the process of PIC micelle formation from flexible PEG-based block cationers and short and rigid siRNAs. Recently, a 14 Lys-PEG (K_{14}-PEG) linear diblock copolymer and siRNA were shown to achieve monomolecular assembly but not the multimolecular assembly that is necessary for PIC micelle formation.[17] In this work, we investigated the formation of PIC micelles incorporating siRNA within the core with hopes of shedding light on the factors affecting the assembly, stability, and efficacy of this novel type of siRNA carrier as a fundamental step in the development of effective PIC-based siRNA delivery systems.

It is assumed that siRNA is more difficult to incorporate in PIC micelle structures than plasmid DNA and oligo-DNA because siRNA is $<^1/_{100}$ the length of plasmid DNA and has more restricted conformational freedom than single-stranded oligo-DNA. Therefore, structural refinement of the polycations used for complexation may improve micelle formation and stability for delivery systems of short and rigid siRNA. Whereas increased stability in biological milieu is needed to allow PIC micelles to reach their target, PIC micelles are also required to release siRNA promptly in the cytoplasm of the target cell for recruitment of siRNA into RNAi machinery. Thus, ideal PIC micelles for siRNA delivery must meet the following rather conflicting requirements: stability of PIC micelles in extracellular media with efficient release of free siRNA from their interior to the cytoplasm of target cells.

In our previous study, poly(ethylene glycol)-*block*-poly(L-lysine) (PEG-*b*-PLL) copolymers were modified to contain thiol groups using *N*-succinimidyl 3-(2-pyridyldithio)propionate (SPDP) to construct PIC micelles with a disulfide cross-linked core for the delivery of plasmid DNA and antisense oligo-DNA.[18−21] The disulfide cross-links are stable under nonreductive physiological conditions contributing to the maintenance of micellar structure and then cleave under reductive conditions following cellular uptake. Disulfides are expected to cleave in the cytoplasm because of elevated levels of glutathione (50−1000 times higher than that in extracellular media[22]). Hence, PIC micelles containing disulfide cross-links within the core may provide the needed stability tradeoff: increased stability in extracellular environment and prompt release of cargo molecules inside the target cell through the cleavage of disulfide bonds. Indeed, plasmid-DNA-loaded PIC micelles comprising a disulfide cross-linked core showed appreciable gene expression in the liver after intravenous administration to mice.[21]

Here we report a novel micellar system for siRNA delivery on the basis of the strategy of core cross-linking via disulfide formation to exert selective release of free siRNA in intracellular milieu while protecting siRNA in extracellular milieu from degradation and nonspecific clearance. PEG-*b*-PLL copolymer was reacted with 2-iminothiolane to obtain poly(ethylene glycol)-*block*-poly[L-*N*-(1-imino-4-mercaptobutyl)lysine] [PEG-*b*-(PLL-IM)] with a portion of lysine residues bearing both mercaptopropyl and amidine groups. This thiolated copolymer was subsequently used to prepare disulfide cross-linked PIC micelles incorporating siRNA. The combination of disulfide cross-links and cationic amidine groups were found to contribute to the increase in the stability of the micelles. Importantly, PIC micelles from PEG-*b*-(PLL-IM) achieved 100-fold higher siRNA activity compared with those from unmodified PEG-*b*-PLL. Such remarkable siRNA activity was correlated with the formation of core−shell-type PIC micelles at critical mixing ratios of block copolymers and siRNA.

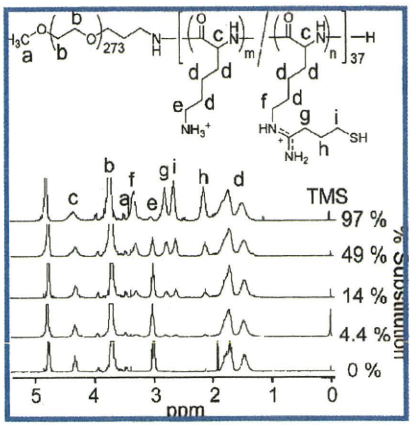

Figure 1. ^{1}H NMR spectra of PEG-*b*-(PLL-IM). Solvent, D_2O; temperature, 25 °C; concentration, 10 mg/mL.

Materials and Methods

Reagents. Dimethyl sulfoxide (DMSO), diethyl ether, dithiothreitol (DTT), D_2O, LiCl, and 2-iminothiolane were purchased from Wako Pure Chemical Industries (Osaka, Japan). Dulbecco's modified Eagle's medium (DMEM), *N*,*N*-diisopropylethylamine (DIPEA) and *N*-methylpyrrolidone (NMP) were purchased from Sigma-Aldrich (St. Louis, MO). Dual-luciferase reporter assay system and pGL3-control and pRL-CMV vectors were purchased from Promega (Madison, WI). Hoechst 33342 was obtained from Dojindo Laboratories (Kumamoto, Japan). SYBR Green II was purchased from Takara Bio (Shiga, Japan). Lipofectamine2000 was purchased from Invitrogen (Carlsbad, CA). siRNA and Cy5-labeled siRNA were synthesized by Dharmacon (Lafayette, CO) and Nihon Bioservice (Saitama, Japan), respectively. The sequences of siRNA against *Photinus pyralis* luciferase were as follows: sense 5′-CUUACGCUGAGUACUUCGAdTdT-3′, antisense 5′-UCGAAGUACUCAGCGUAAGdTdT-3′.

Synthesis of PEG-*b*-(PLL-IM). PEG-*b*-PLL copolymer (M_w of PEG: 12 000; polymerization degree of PLL: 37; M_w/M_n: 1.08) was synthesized as previously described.[20,23] Iminothiolane modification of PEG-*b*-PLL was achieved by reacting primary amino groups in side chains of PLL segments with 2-iminothiolane. First, PEG-*b*-PLL (37.5 mg/mL) and 2-iminothiolane (25 mg/mL) were separately dissolved in NMP containing 5 wt % LiCl. Then, the solutions were mixed at various molar ratios of 2-iminothiolane/Lys up to 2.0 and stirred at 25 °C for 18 h after the addition of DIPEA (5 equiv relative to lysine (Lys) units). The mixtures were purified by precipitation in a 15-fold excess of diethyl ether (60 mL). Precipitated polymer was redissolved in 0.01 N HCl (20 mL), dialyzed against distilled water (MWCO: 2000), and lyophilized to obtain pure PEG-*b*-(PLL-IM) copolymer. The products were subjected to ^{1}H NMR analysis in D_2O using a 300 MHz spectrometer (EX 300, JEOL, Tokyo, Japan). The degree of substitution for each PEG-*b*-(PLL-IM) was determined from the ^{1}H NMR spectra shown in Figure 1 by the peak intensity ratio of the β-, γ-, and δ-methylene protons of Lys ($(CH_2)_3$, $\delta = 1.3$ to 1.9) to the protons of trimethylene units of mercaptopropyl groups ($HS-(CH_2)_3$, $\delta = 2.1$ to 2.8). The calculated substitution degrees are shown as PEG-*b*-(PLL-$IM_{x\%}$) where x stands for the percent substitution.

Preparation of Disulfide Cross-Linked Polyion Complex Systems. Before complexation with siRNA, PEG-*b*-(PLL-IM) solutions were incubated in a DTT solution (100 mM in 10 mM HEPES−NaOH, pH 7.4) at 25 °C for 30 min to reduce any disulfide bonds. Then, polymer solution was added to a two-fold excess volume of 15 μM siRNA (600 mM phosphate groups of siRNA) solution at different mixing ratios to form PICs. The mixing ratio for each complexation study was determined by N/P: [primary amines and amidines of block copolymers]/[phosphate groups of siRNA]. After overnight incubation at 25 °C, thiol groups were oxidized to form disulfide cross-links by dialysis against 10 mM HEPES−NaOH buffer (pH 7.4) containing 0.5%

DMSO at 37 °C for 2 days, followed by 2 days of additional dialysis against 10 mM HEPES−NaOH buffer (pH 7.4) for the removal of DMSO. To confirm oxidation, remaining free thiol groups were quantified using Ellman's method.[24]

Measurement of Scattered Light Intensity, Size, and ζ Potential of Polyion Complexes. PICs formed from PEG-*b*-(PLL-IM) and siRNA were evaluated by static (SLI) and dynamic (DLS) light scattering measurements before and after the removal of DTT from the complexation milieu: the former measurement was carried out to examine the effect of the mixing ratios on the formation of PIC assemblies, whereas the latter measurement was aimed to evaluate the stability and environment responsiveness of the disulfide cross-linked systems. All light scattering measurements were carried out using a Zetasizer Nano ZS (Malvern Instruments, Malvern, UK) equipped with a He−Ne laser (λ = 633 nm) as the incident beam. In DLS measurements, size distributions were determined by cumulant and histogram analysis, and results are shown as the z-average size (cumulant mean) with polydispersity index (PDI) (defined in the ISO standard document 13 321:1996) and the histogram of size distribution. Briefly, cumulant analysis was performed by expanding the logarithm of the normalized correlation function $g^{(1)}(t)$ as a power series in the time t

$$\ln[g^{(1)}(t)] = -K_1 t + (1/2)K_2 t^2 + \ldots$$

yielding an average of the reciprocal relaxation time, K_1, and PDI, K_2/K_1^2. K_1 was further converted to a translational diffusion coefficient to calculate the z average by using the Stokes−Einstein equation. The ζ potentials of the complexes were measured in 10 mM HEPES−NaOH buffer (pH 7.4) containing 150 mM NaCl at 37 °C. All samples were equilibrated to the defined temperature for 24 h prior to measurement.

Gel Retardation Analysis. Non-cross-linked PICs prepared in reductive milieu as described above were electrophoresed at 100 V for 1 h on 20% polyacrylamide gel in tris-borate EDTA buffer (100 mM Tris, 90 mM boric acid, 1 mM EDTA) to qualitatively determine if free siRNA remained after polymer complexation. The gel was stained with SYBR Green II according to the manufacturer's protocol and visualized using a UV transilluminator.

Stability of Polyion Complexes. The effect of cross-linking on PIC stability was determined as a function of NaCl concentration using a Zetasizer Nano ZS (Malvern Instruments, Malvern, UK). The assay was performed by measuring the scattering light intensity (SLI) of PICs after 24 h of incubation at 37 °C in solutions containing different NaCl concentrations ranging from 75 to 600 mM NaCl. PIC size distribution was also obtained by histogram analysis of DLS measurement.

Atomic Force Microscopy Analysis. Disulfide cross-linked PIC assemblies were visualized by AFM imaging. For each analysis, sample solution (4 μL) was deposited onto a freshly cleaved mica substrate for 30 s, and the solution was dried under a gentle flow of nitrogen. AFM imaging was performed in tapping mode with standard silicon probes (125 μm in length, Veeco Instruments, CA) on a nanoscope (Veeco Instruments). The cantilever oscillation frequency was tuned to the resonance frequency of the cantilever, 200−400 kHz. Raw AFM images have been processed for only background removal (flattening) using the microscope manufacturer's image-processing software.

siRNA Transfection. Huh7 cells (human hepatoma cells) were plated onto 24-well culture plates (2×10^4 cells/well), followed by 20 h of incubation in DMEM containing 10% fetal bovine serum (FBS). Then, 360 ng/well pGL3-control, encoding *Photinus pyralis* luciferase (Pp-Luc), and 40 ng/well pRL-CMV, encoding *Renilla reniformis* luciferase (Rr-Luc), plasmid DNA were applied with Lipofectamine2000 according to the manufacturer's instructions, and cells were further incubated for 4 h to allow transfection of plasmid DNAs. The medium was replaced, and PICs with or without disulfide cross-linking were applied to each well for transfection of siRNA (1−500 nM) against Pp-Luc. After 48 h, cells were rinsed with PBS and subjected to a luciferase expression assay using the dual-luciferase reporter assay system. For each assay, Pp-Luc and Rr-Luc luminescence was measured using a Mithras LB940 plate reader (Berthold Technologies, Bad Wildbad, Germany) after the addition of appropriate substrates. Pp-Luc activities were normalized by Rr-Luc activities, and values are expressed as a ratio to the control value (mean ± SD, n = 4).

Flow Cytometry. Huh7 cells were plated onto six-well culture plates, followed by 24 h of incubation in DMEM containing 10% FBS. The medium was replaced, and Cy5-siRNA-incorporated PICs with or without disulfide cross-linking were applied (100 nM siRNA) to each well. After 1 h, cells were rinsed three times with PBS and collected by trypsinization. The collected cells were centrifuged at 100*g* for 2 min and resuspended in PBS. The fluorescence intensity was detected and acquired using a BD LSR II instrument (BD Biosciences, Franklin Lakes, NJ) equipped with FACS Diva software (BD Biosciences). Detection of Cy5 fluorescence was achieved using a 633 nm He−Ne laser for excitation, and a 660/20 band-pass filter for emission.

Confocal Laser Scanning Microscopy. Huh7 cells were seeded onto 35 mm glass-bottomed Petri dishes, followed by 24 h of incubation in DMEM containing 10% FBS. The medium was replaced, and Cy5-siRNA-incorporated PICs with or without disulfide cross-linking were applied at 100 nM siRNA to each dish. After 3 h, cells were stained with Hoechst 33342 according to the manufacturer's protocol and were then rinsed three times with PBS and observed by confocal laser scanning microscopy (CLSM) under fresh culture medium. CLSM observation was performed using a LSM 510 (Carl Zeiss, Oberkochen, Germany) microscope equipped with a 63× objective (C-Apochromat, Carl Zeiss). Detection of Cy5 and Hoechst 33342 fluorescence was achieved using 633 nm He−Ne and 710 nm Mai Tai lasers for excitation, and 651−704 nm and 390−465 nm band-pass filters for emission, respectively.

Results

Preparation of PEG-*b*-(PLL-IM). Primary amines in lysine residues of PEG-*b*-PLL readily reacted with the cyclic imidoester 2-iminothiolane via a ring-opening reaction, generating mercaptopropyl groups through amidine bonds to obtain PEG-*b*-(PLL-IM).[25] In ^{1}H NMR measurements, the transformation of primary amines to amidines was evident: the ε-methylene protons of lysine residues were shifted downfield (e to f, Figure 1) in addition to the appearance of proton signals characteristic to the CH_2 units of γ-mercapto-propyl groups (g−i, Figure 1). The degree of substitution was calculated from these characteristic signals, as described in the Materials and Methods section. By changing the feed ratios of 2-iminothiolane to primary amino groups of PEG-*b*-PLL, a series of PEG-*b*-(PLL-IM) with varying degrees of substitution was obtained in good yield (71−90%). The reactions at feed ratios (2-iminothiolane/primary amine) of 0.15, 0.6, 1, and 2 resulted in 14, 48, 69, and 97% substitutions, respectively.

Formation of Polyion Complexes from PEG-*b*-(PLL-IM) and siRNA. PEG-*b*-(PLL-IM) copolymer solutions were mixed with siRNA at varying N/P ratios under reductive conditions to form the desired PICs. PIC formation was confirmed by the observation of increased scattered light intensity (SLI), which is correlated to the product of molar concentration and squared molecular weight of the analytes. Of interest, the SLI of each PIC solution reached a maximum at a specific N/P ratio, which varied depending on the substitution degree of PEG-*b*-(PLL-IM) (Figure 2). For example, the PEG-*b*-PLL system showed a maximum SLI at N/P = 1.2, and a subtle change in N/P induced a drastic decrease in the SLI, indicating that PICs formed from PEG-*b*-PLL assembled into higher ordered micelle structures only at N/P = 1.2. Likewise, a critical N/P ratio for the formation of higher order large PIC assemblies was found for each PEG-*b*-(PLL-IM) except for PEG-*b*-(PLL-IM$_{97\%}$), in which the SLI continuously increased to N/P = 7.

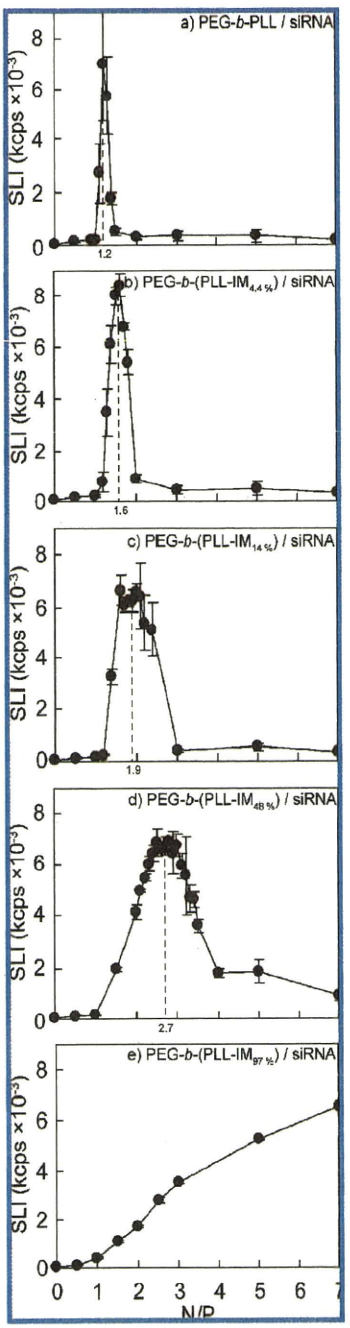

Figure 2. Static light scattering analysis of PIC assemblies formed from PEG-*b*-(PLL-IM)s and siRNA at various N/P ratios under reductive conditions. Scattered light intensity (SLI) was recorded at 25 °C in 10 mM HEPES–NaOH buffer (pH 7.4) containing 33 mM DTT. Values are expressed as the mean ± SD, $n = 3$.

The size distributions of the PICs formed at the characteristic N/P ratio that gives a maximum SLI in Figure 2 were analyzed by DLS. Curiously, the autocorrelation curve of PIC assemblies formed from PEG-*b*-PLL and siRNA exhibited complicated and slow decay that was out of the range of particle size analysis by DLS (data not shown). The PEG-*b*-PLL system might not form a simple spherical micellar structure as suggested in the result of histogram analysis (Figure 3a). In contrast, PIC assemblies formed from siRNA and PEG-*b*-(PLL-IM) with >14% substitution showed narrow size distributions with PDI < 0.045 and diameters ranging from 40 to 58 nm, depending

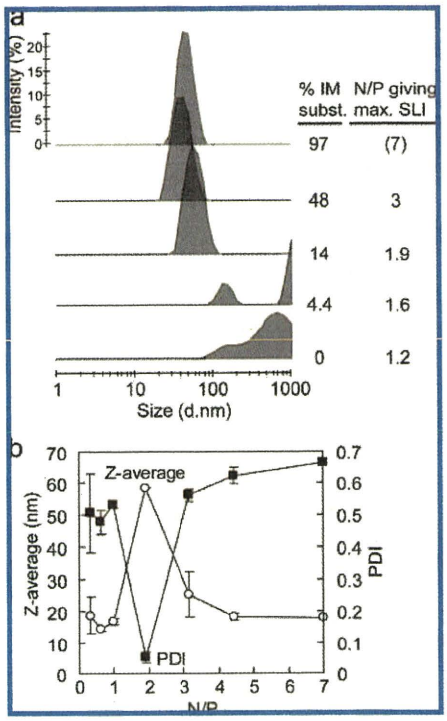

Figure 3. Dynamic light scattering analysis of PIC assemblies formed from PEG-*b*-(PLL-IM) and siRNA under reductive conditions. (a) Size distributions of the PIC assemblies formed at the N/P ratio of each maximum of SLI. (b) N/P dependency of size distributions of the complexes formed from PEG-*b*-(PLL-$IM_{14\%}$) and siRNA. All measurements were performed at 25 °C in 10 mM HEPES–NaOH buffer (pH 7.4) supplemented with 33 mM DTT.

on the substitution degree (Figure 3a and Supporting Information). These size and PDI values are consistent with the formation of spherical micelles with core–shell architecture in which the PIC core of siRNA and PLL-IM is surrounded by a PEG shell. Note that even for PEG-*b*-(PLL-IM)s, a deviation in the N/P ratios from the critical value resulted in a significant increase in PDI values accompanied by decreased SLI, which suggests a transformation to less-ordered micelle structures with a lower association number. A typical N/P dependency of PDI and size distribution for PICs formed from PEG-*b*-(PLL-$IM_{14\%}$) and siRNA is shown in Figure 3b, indicating that narrowly distributed PIC micelles with a size that was consistent with the core–shell model were formed only at the characteristic point (N/P = 1.9) where the SLI also showed a maximum value (Figure 2).

The incorporation of siRNA into PIC assemblies was confirmed by polyacrylamide gel electrophoresis (Figure 4). Interestingly, free siRNA was not observed above the critical N/P mixing ratios shown in Figure 2 for all of the samples with 0 to 69% substitution degree, indicating the stable association of siRNA into PICs above the critical N/P ratio but not organized micelle structures as the SLI decreased substantially. As for the sample with 97% substitution degree [PEG-*b*-(PLL-$IM_{97\%}$)], a migrative fraction of siRNA could not be detected above the N/P ratio of 4.

Characterization of Disulfide Cross-Linked Polyion Complex Assemblies. Multimolecular PIC assemblies, defined as PIC micelles, formed from siRNA and PEG-*b*-(PLL-IM) prepared at the critical N/P ratio under reductive conditions were subsequently dialyzed against 10 mM HEPES–NaOH buffer (pH 7.4) containing 0.5% DMSO to form disulfide cross-links

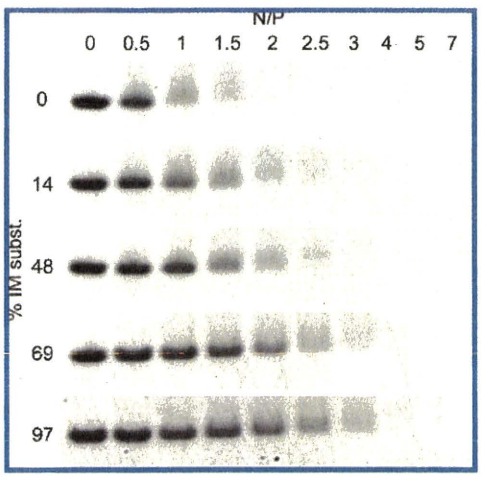

Figure 4. Gel retardation analysis of siRNA complexed with PEG-*b*-(PLL-IM)s under reductive conditions. Free siRNA was stained with SYBR Green II and visualized using a UV transilluminator.

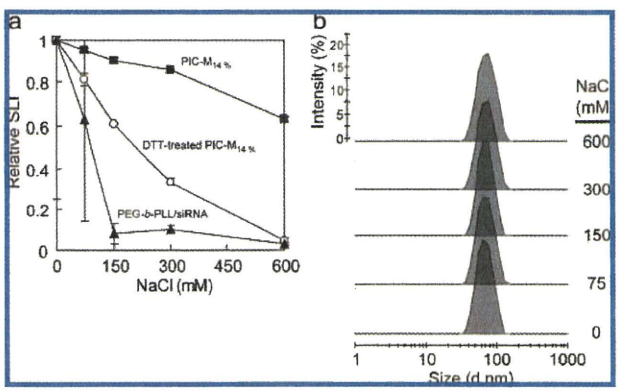

Figure 5. Stability and environment responsiveness of disulfide cross-linked micelles. (a) Scattered light intensity of PIC-$M_{14\%}$, DTT-treated PIC-$M_{14\%}$, and PIC assemblies from PEG-*b*-(PLL)/siRNA with increased concentration of NaCl. (b) Size distributions of PIC-$M_{14\%}$ at each NaCl concentration.

through the oxidation of thiol groups. After dialysis, the amount of residual thiol groups was determined to be <10% of the initial value for all of the samples, indicating that the core of the PIC-Ms were successfully cross-linked through disulfide bonds. (See the Supporting Information.) Hereafter, siRNA-incorporated PIC micelles prepared from PEG-*b*-(PLL-$IM_{x\%}$) are abbreviated as PIC-$M_{x\%}$.

The stability of PIC assemblies against ionic strength was evaluated by SLI and DLS measurements at various NaCl concentrations. As seen in Figure 5a, there was a significant decrease in SLI for the PEG-*b*-PLL/siRNA system with an increase in NaCl concentration, indicating that the system is highly sensitive to ionic strength, and cannot tolerate physiological salt concentration. Alternatively, PIC-$M_{14\%}$ cross-linked micelles retained >80% of their initial SLI value at 300 mM NaCl and retained 60% of their initial SLI value even at a NaCl concentration as high as 600 mM. Cumulant analysis of DLS measurements at various NaCl concentrations revealed that the PIC-$M_{14\%}$ maintained an almost constant diameter (~70 nm by z average) with very narrow distribution (PDI < 0.067) up to 600 mM NaCl. (See the Supporting Information.) Histogram analysis of DLS measurement further corroborated the stable and narrow size distribution of PIC-$M_{14\%}$ against an increase in NaCl concentration, as shown in Figure 5b.

Table 1. ζ Potentials of Disulfide Cross-Linked Micelles

% IM subst.	N/P giving max SLI	ζ potential (mV) (mean ± SD)
0	1.2	−2.6 ± 1.3
4.4	1.6	−0.73 ± 0.44
14	1.9	−2.4 ± 1.1
49	3	−1.4 ± 2.1
69	3.9	−0.73 ± 0.15

The stability of PIC-$M_{14\%}$ at different NaCl concentrations was also evaluated by SLI after the addition of DTT, which aimed to cleave disulfide cross-linking in the core and disrupt micelle stability. As seen in Figure 5a, the addition of DTT to PIC-$M_{14\%}$ solution induced a significant decrease in the SLI with increasing NaCl concentration (Figure 5a, ○). This result indicates the critical role of disulfide cross-links in the improved stability of PIC micelles against increased ionic strength as well as the feasibility of dissociation of cross-linked micelles under reductive conditions and physiological ionic strength, such as the intracellular environment.

Table 1 shows the ζ potential of PIC-$M_{x\%}$ formed at the critical N/P ratio depending on the substitution degree in 10 mM HEPES−NaOH (pH 7.4) containing 150 mM NaCl at 37 °C. Data for a PEG-*b*-PLL/siRNA system formed at the critical N/P ratio of 1.2 are also shown as a control. The ζ potential varied only slightly from −2.6 to −0.73 mV, regardless of micelle composition. Furthermore, these small absolute values of ζ potential remained unchanged even after the storage of cross-linked PIC-Ms in solution for several months. (See the Supporting Information.) The stable and electrostatically neutralized PIC-Ms in the stored solution are consistent with the formation of a core−shell structure where the PEG shell prevents micelle aggregation through decreased interfacial free energy as well as increased steric repulsion.

The morphology of PIC assemblies was directly observed by AFM, as shown in Figure 6. PIC-$M_{48\%}$ had a spherical shape with a diameter of ~50 nm, which is consistent with the formation of polymeric micelles. There was no change in the size and morphology even after incubation in medium containing 150 mM NaCl. Taken together with the data from light scattering analyses, it is reasonable to conclude that a stable disulfide cross-linked PIC micelle was formed from PEG-*b*-(PLL-IM)s and siRNA at the N/P ratio coinciding with maximum SLI intensity.

siRNA Transfection Using Disulfide Cross-Linked Micelles. A series of disulfide cross-linked micelles composed of PEG-*b*-(PLL-IM) with various substitution degrees, PIC-$M_{x\%}$, were evaluated as carriers for siRNA in cultured cells. In this experiment, Huh7 cells were transiently transfected with the reporter genes Pp-Luc and Rr-Luc, followed by the treatment with PIC-$M_{x\%}$ prepared at the appropriate N/P ratio containing siRNA against Pp-Luc. After a transfection period of 48 h, the inhibition of Pp-Luc expression was evaluated by measuring the relative expression of Pp-Luc/Rr-Luc. First, we examined the siRNA transfection efficacy of disulfide cross-linked micelles formed from PEG-*b*-(PLL-IM) with different substitution degrees (PIC-$M_{x\%}$) at a concentration of 100 nM siRNA. Ultimately, PIC-$M_{14\%}$ was found to achieve the highest silencing efficacy of Pp-Luc gene (Figure 7a). The system with higher and lower substitution degrees than PIC-$M_{14\%}$ resulted in lower siRNA transfection efficacy. We then evaluated the dose-dependent siRNA transfection efficiencies of PIC-$M_{14\%}$ in comparison with naked siRNA and non-cross-linked PIC assemblies from PEG-*b*-PLL as controls. PIC-$M_{14\%}$ had an ED_{50} (defined as the siRNA concentration required to induce 50% of

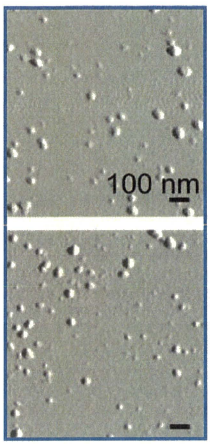

Figure 6. AFM images of disulfide cross-linked micelles (PIC-$M_{48\%}$). Images were acquired before (upper) and after (lower) incubation in 150 mM NaCl.

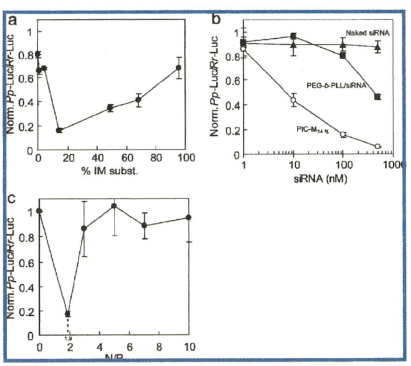

Figure 7. Disulfide cross-linked micelle-mediated siRNA transfection. (a) 100 nM siRNA was transfected in Huh7 cells with disulfide cross-linked micelles. Each of the micelles was prepared from PEG-*b*-(PLL-IM) and siRNA at the optimal N/P maximum in SLI. (b) Dose-dependent knockdown by PIC-$M_{14\%}$ compared with naked siRNA and non-cross-linked PIC assemblies from PEG-*b*-PLL and siRNA. (c) N/P dependency of the knockdown efficiency of the disulfide cross-linked complexes formed from PEG-*b*-(PLL-$IM_{14\%}$) and siRNA. Values are expressed as the mean ± SD, $n = 4$.

gene knockdown) that was approximately two orders of magnitude lower than that of PIC assemblies of PEG-*b*-PLL, which indicates a significant improvement in siRNA transfection efficacy by the introduction of disulfide cross-links to the PIC-M structure (Figure 7b). The effect of N/P ratios used to form cross-linked assemblies from PEG-*b*-(PLL-$IM_{14\%}$) on siRNA transfection efficacy was also evaluated. As shown in Figure 7c, effective siRNA transfection was achieved at only the critical N/P ratio of 1.9, where the PIC assembled in the micellar structure, as seen in Figures 2 and 3b. Apparently, the formation of micellar structure is well correlated with siRNA transfection efficiency. The siRNA transfection efficacy of Lipofectamine2000 was also determined using the dual luciferase assay for comparison with micellar systems. A significant decrease in Pp-Luc (Pp-Luc/Rr-Luc = 0.03 at 100 nM siRNA) was accompanied by a significant decrease in Rr-Luc expression (>80% lower expression than micellar systems), which indicated Lipofectamine2000 cytotoxicity. (See the Supporting Information.) The cytotoxicity of Lipofectamine2000 prevented a direct comparison with micellar systems under the conditions of this reporter system. Micellar systems showed minimal cytotoxicity at all concentrations used for dual luciferase assay with >75% viability retained at 100 nM siRNA for PIC-$M_{14\%}$. (See the Supporting Information.) Although little is known about the biocompatibility of iminothiolane functional groups, the observed low cytotoxicity in cultured cells is promising and warrants further investigation in vivo to determine the biocompatibility and tolerance of these micellar siRNA delivery systems.

To investigate the transfection properties of PIC micelles in more detail, PICs containing Cy5-labeled siRNA were prepared and applied to Huh7 cells. It should be noted that the incorporation of Cy5-labeled siRNA into micelles resulted in ~75% fluorescence quenching, with no significant shift in absorbance or emission maximum. (See the Supporting Information.) Figure 8a shows flow cytometric analysis (FCM) of Huh7 cells treated with PIC-$M_{14\%}$ and PIC assemblies from PEG-*b*-PLL. We analyzed FCM data by determining the mean fluorescence intensity (MFI) of the cell population. Significantly higher fluorescence (MFI = 5221) was observed for Cy5-siRNA incorporated PIC-$M_{14\%}$ compared with the PIC assembly formed from PEG-*b*-PLL/Cy5-siRNA (MFI = 632) and naked Cy5-siRNA (MFI = 1032). The uptake of free siRNA may appear to be higher than expected because of Cy5 quenching in micelle cores and the presence of hydrophobic dye that may facilitate interaction with cell membrane components and increase uptake. It should be noted that the absolute values of fluorescence intensity are relatively low for all three species, indicating that cellular uptake was not rapid. CLSM of cells treated with PIC micelles containing Cy5-siRNA further supported the data of FCM analysis, as seen in Figure 8b. Whereas the fluorescence of naked Cy5-siRNA or Cy5-siRNA transfected with PEG-*b*-PLL was hardly detectable under the same CLSM configuration as that used for PIC-$M_{14\%}$, 100% of cells transfected with PIC-$M_{14\%}$ gave CLSM images with an intracellular localization of Cy5 fluorescence signal 3 h after transfection. These results demonstrate that the highly efficient knockdown of the Pp-Luc gene by PIC-$M_{14\%}$ was achieved by an effective uptake of siRNA in the cell presumably due to the formation of a stable micellar structure.

Discussion

In this study, we have demonstrated that disulfide cross-linked PIC-Ms appreciably enhanced siRNA transfection. Stable and unimodal micellar formation occurred at a specific mixing ratio (N/P) only when the primary amino groups of PEG-*b*-PLL were at least partially modified with thiol groups through amidine bonds. These disulfide cross-linked micelles exhibited remarkable stability in physiological medium, underwent dissolution upon the reduction of disulfide cross-links to allow the release of entrapped siRNA, and achieved 100 times higher transfection efficiency than PIC assemblies without disulfide cross-links.

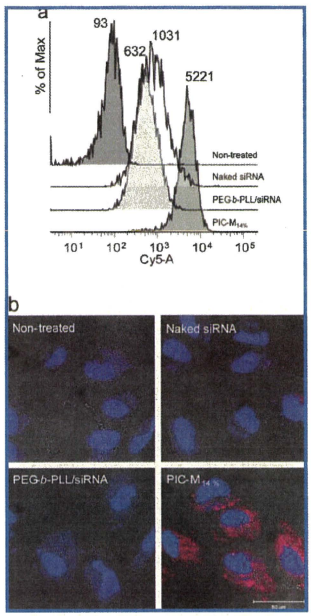

Figure 8. Cellular uptake of Cy5-labeled siRNA transfected with PIC-$M_{14\%}$ or assemblies formed from PEG-*b*-PLL at the N/P of maximum in SLI. (a) Flow cytometric analysis of Huh7 cells 1 h after Cy5-siRNA transfection. Values indicate the mean fluorescence intensity (MFI) of the cell population. Nontreated represents the fluorescence emitted from untreated Huh7 cells. (b) Confocal laser scanning microscopic analysis of Huh7 cells 3 h after Cy5-siRNA (red) transfection. Cell nuclei were stained with Hoechst 33342 (blue).

The assembly of block catiomers and siRNA showed a distinct change in association number governed by the mixing ratio (N/P). The relatively weak SLI obtained from mixed solutions of block catiomer and siRNA at ratios of N/P $\leq$ 1 indicated that few recognizable multimolecular assemblies with increased association number formed (Figure 2). Considering the gradual decrease in the migrative siRNA fraction in PAGE analysis (Figure 4) as well as the moderate SLI when N/P was increased by 1, siRNA excess mixtures might have formed charge−stoichiometric complexes that do not assemble into micelle-like multimolecular assembly. However, at the very specific N/P typically slightly above 1, SLI showed a dramatic increase, suggesting the successful formation of multimolecular assemblies. Although, possibly due to incomplete protonation of PEG-*b*-PLL lysines ($pK_a \approx 9.5$, ~95% protonation at pH 7.3),[23,26] N/P maxima did not precisely correspond to the equal charge ratios of siRNA and block catiomer; controlled excess of catiomer appeared to be crucial for micellar assembly. A likely explanation of the mechanism of this distinct assembling behavior is that a slight excess amount of block catiomers assists multimolecular assembly through intermolecular ion bridging. It should be noted that multimolecular assembly was abrogated with a further increase in N/P, as seen by the steep decrease in SLI and increase in PDI (Figures 2 and 3b), even though stable complexation of block catiomer and siRNA was strongly suggested by the absence of migrative siRNA upon gel electrophoresis of samples prepared above the characteristic N/P that gives maximum SLI (Figure 4). In the block catiomer−large excess mixture, the multimolecular assembly could have been hindered by the electrostatic repulsion between catiomer−excess small complexes or steric inconsistency, which is characteristic of block copolymers, as previously described.[27]

Recent experiments with PEGylated polyelectrolyte systems containing PEG-*block*-poly(aspartate) (PEG-*b*-PAsp), PEG-*b*-PLL, and PLL show that assembly behavior is influenced by a variety of factors including polyion chain length and the presence of homopolymer.[27] This study demonstrated that block copolymer acts as the host molecule in PICs and that PEGylation of polyions may change the complexation process from loose noncooperative association to tight cooperative pairing, in turn leading to growth into stoichiometric core−shell PIC micelles with an appreciably high association number.

In the study described above, light scattering intensity increased to an optimum upon mixing of PEG-*b*-PAsp with increasing ratios of PLL, whereas the size underwent a sharp drop in the region with excess PLL because in this range, all PEG-*b*-PAsp chains behave as host molecules to participate in complexation with PLL as a guest molecule, leading to a decreased association number as a result of steric inconsistency. This scheme may also be valid for siRNA complexation, with excess block catiomer inducing a steep drop in association number.

It is interesting that the characteristic mixing ratio where the multimolecular assembly of block catiomer and siRNA occurred shifted to higher N/P with increased IM content. We further investigated this assembly behavior by recalculating N/P ratios in SLI experiments and neglecting the charge contribution from IM groups. (See the Supporting Information.) Multimolecular assembly of PEG-*b*-(PLL-$IM_{0-69\%}$) and siRNA was achieved at 1.2 to 1.5 by the ratio of [unmodified Lys primary amine]/[siRNA phosphate]. It is reasonable to assume that the relatively long-range Coulomb interaction between oppositely charged primary amines and phosphates is the dominant driving force that contributes to multimolecular assembly. However, the monodispersity of multimolecular assemblies was clearly improved with the increased degree of IM substitution (Figure 3a), which might be explained by the chemistry of the amidine bonds of IM groups. Phosphates and amidine analogs such as the guanidino bond in IM groups form relatively strong hydrogen bonds in addition to ionic interactions.[28] This interaction is crucial for strong association of guanidinium groups with phosphates because it was recently shown that methylation of arginine groups and elimination of hydrogen-bonding capability greatly reduced the activity and insertion ability of a short arginine-rich membrane-active peptide toward a phospholipid membrane.[29] It should be noted that hydrogen bond formation requires close contact of proton donors and acceptors, and its contribution can be dramatically reduced in a solvent with a high dielectric constant, such as water.[30] Multimolecular assembly would allow close contact of polymer chains, with the core being rather hydrophobic compared with the exterior medium, and would therefore be favorable for hydrogen bond formation. Thus, initial multimolecular assembly may be driven by long-range electrostatic interaction of primary amines and siRNA phosphates with amidine−phosphate short-range interactions, resulting in a more ordered and uniform micelle core structure. Amidine functional groups might have facilitated unimodal multimolecular assembly of PEG-*b*-(PLL-IM) and

Scheme 1. Preparation of Iminothiolane-Modified Poly(ethylene glycol)-*block*-poly(L-lysine) [PEG-*b*-(PLL-IM)]

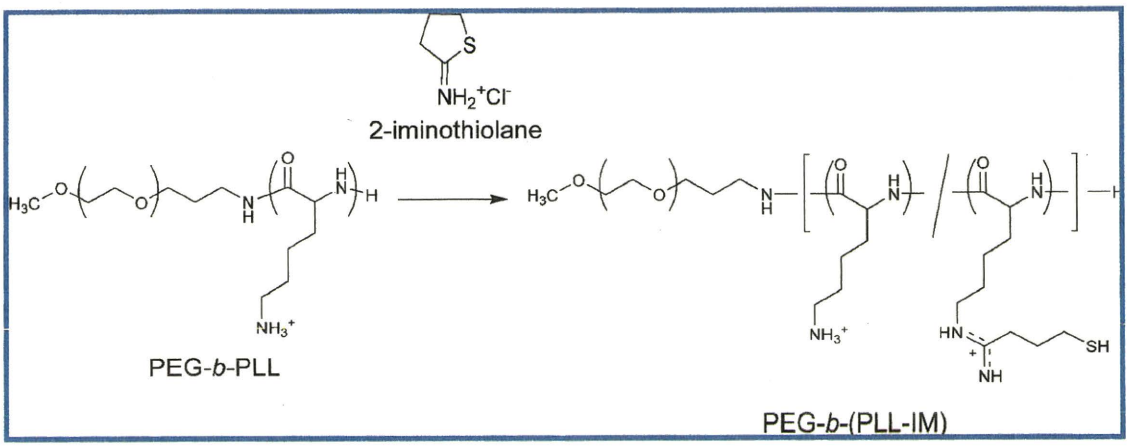

siRNA through intrinsic interaction modes, which are distinct from that of primary amines in unmodified lysines. Additionally, the presence of sulfur-containing side chains in the block copolymer may have also affected the formation of monomodal multimolecular assemblies because of increased hydrophobicity or restriction of the possible orientations to accommodate bulky groups in the micelle core. Interestingly, PIC-Ms formed between PEG-*b*-PLL modified with the sulfur-containing cross-linker N-succinimidyl 3-(2-pyridyldithio)-propionate (SPDP) and siRNA also showed a decrease in size and dispersity with increased thiol modification degree. (See the Supporting Information.) The detailed mechanism of monomodal micelle formation between block copolymer cations and siRNA remains elusive and requires more work to elucidate the interesting assembly behavior observed in this work.

The most important achievement of this work was the identification of the factors required to form unimodal multimolecular assemblies between IM-modified cationic block copolymers and siRNA, yielding siRNA-incorporated disulfide cross-linked PIC-Ms that accomplished highly efficient siRNA transfection. Amidine groups of PEG-*b*-(PLL-IM) were strongly suggested to facilitate unimodal micellar assembly with siRNA, as discussed above, whereas thiols were shown to confer environment responsiveness to resulting PIC micelles through the formation of disulfide cross-links within their cores (Figure 5a). Another important finding was the strong correlation between transfection efficiency and the formation of micellar structure. Even in the disulfide cross-linked system, efficient transfection was achieved only at the critical N/P for micelle formation, a slight deviation from the optimal N/P resulted in a sharp drop in transfection efficacy (compare Figures 2, 3b, and 7c). Resistance of siRNA to enzymatic degradation is not the major reason for this unique property of PIC-Ms because nonmicellar complexes of PEG-*b*-PLL and siRNA formed at N/P = 2 showed appreciable stabilization of siRNA in 70% FBS medium even after 24 h of incubation. (See the Supporting Information.) Apparently, as seen in Figure 8, the incorporation of siRNA in cross-linked PIC-Ms significantly improved cellular uptake, leading to a remarkable gene silencing effect for the micelle composition with optimal cross-linking density.

Conclusions

In this study, we established a method for preparing disulfide cross-linked PIC-Ms from PEG-*b*-(PLL-IM) and siRNA. The formation of PIC-Ms was strictly controlled by the mixing ratio of the block copolymer with siRNA, yielding monodisperse PIC-Ms at only specific N/P ratios. Disulfide cross-linking contributed to the stabilization of otherwise fragile PIC-Ms under physiological salt conditions. Careful tuning of IM modification imparted environmental responsivity of PIC-Ms to reductive conditions, allowing the prompt release of encapsulated siRNA. Effective silencing of the target gene was demonstrated in cultured cells by siRNA-incorporated PIC-Ms with controlled cross-linking density. These results show the promise of PIC-Ms as a building block for the development of highly effective siRNA delivery systems.

Acknowledgment. This study was supported by Special Coordination Funds for Promoting Science and Technology (SCF) commissioned by the Ministry of Education, Culture, Sports, Science, and Technology (MEXT) of Japan.

Supporting Information Available. A summary of size and PDI of PIC-Ms formed with PEG-*b*-(PLL-IM) of various IM compositions and siRNA, residual thiol content of cross-linked PIC-Ms formed with PEG-*b*-(PLL-IM)s and siRNA, size and PDI of PEG-*b*-PLL(IM) PIC-Ms prepared at each optimal N/P at various NaCl concentrations, PIC-$M_{14\%}$ stability versus time, Lipofectamine2000 siRNA transfection efficacy, PIC-$M_{14\%}$ and PEG-*b*-PLL/siRNA PIC cytotoxicity, Cy5 fluorescence quenching after incorporation into PIC-$M_{14\%}$, SLI measurements plotted as a function of the N/P ratio of unmodified primary amines, PEG-*b*-PLL(PDP) structure and corresponding PIC-M properties, and stability of siRNA incorporated PEG-*b*-(PLL-IM) PIC-Ms toward enzymatic degradation are available. This material is available free of charge via the Internet at http://pubs.acs.org.

References and Notes

(1) Elbashir, S. M.; Harborth, J.; Lendeckel, W.; Yalcin, A.; Weber, K.; Tuschl, T. *Nature* **2001**, *411*, 494–498.
(2) Fire, A.; Xu, S. Q.; Montgomery, M. K.; Kostas, S. A.; Driver, S. E.; Mello, C. C. *Nature* **1998**, *391*, 806–811.
(3) Behlke, M. A. *Mol. Ther.* **2006**, *13*, 644–670.
(4) de Fougerolles, A.; Vornlocher, H.-P.; Maraganore, J.; Lieberman, J. *Nat. Rev. Drug Discovery* **2007**, *6*, 443–453.
(5) Morrissey, D. V.; Lockridge, J. A.; Shaw, L.; Blanchard, K.; Jensen, K.; Breen, W.; Hartsough, K.; Machemer, L.; Radka, S.; Jadhav, V.; Vaish, N.; Zinnen, S.; Vargeese, C.; Bowman, K.; Shaffer, C. S.; Jeffs, L. B.; Judge, A.; MacLachlan, I.; Polisky, B. *Nat. Biotechnol.* **2005**, *23*, 1002–1007.
(6) Soutschek, J.; Akinc, A.; Bramlage, B.; Charisse, K.; Constien, R.; Donoghue, M.; Elbashir, S.; Geick, A.; Hadwiger, P.; Harborth, J.; John, M.; Kesavan, V.; Lavine, G.; Pandey, R. K.; Racie, T.; Rajeev, K. G.; Rohl, I.; Toudjarska, I.; Wang, G.; Wuschko, S.; Bumcrot, D.;